Characterization of Starch Nanoparticles by Fluorescence Techniques

by

Wei Yi

A thesis

presented to the University of Waterloo

in fulfillment of the

thesis requirement for the degree of

Master of Science

in

Chemistry

Waterloo, Ontario, Canada, 2014

AUTHOR'S DECLARATION

I hereby declare that I am the sole author of this thesis. This is a true copy of the thesis, including any required final revisions, as accepted by my examiners.

I understand that my thesis may be made electronically available to the public.

Abstract

The properties of starch nanoparticles (SNPs) labeled with the fluorescent dye pyrene (Py-SNPs) were probed by using fluorescence quenching, pyrene excimer formation, and transmission electron microscopy (TEM). Pyrene labeling of the SNPs was achieved by reacting 1-pyrenebutyric acid with the hydroxyl groups of the SNPs under basic conditions and in the presence of diisopropylcarbodiimide. This procedure did not degrade the SNPs as confirmed by dynamic light scattering (DLS) and afforded a means to generate a pyrene labeling level ranging from 0.5 to 5.0 mol% of the glucose units making up the SNPs. A polymeric quencher was also synthesized to probe the accessibility of the interior of the Py-SNPs by using fluorescence quenching measurements. The polymeric quencher was a 2K poly(ethylene glycol) terminated at one end with a methyl group and a nitropropane group at the other. Unfortunately these quenching experiments were abandoned when it was found that the polymeric quencher synthesized for these experiments absorbed too strongly where pyrene absorbs. Intramolecular pyrene excimer formation in the Py-SNPs was investigated by steady-state and time-resolved fluorescence. These experiments demonstrated that the Py-SNPs contract but do not overlap like linear polymers do in the semi-dilute regime. They also showed that despite the inherent rigidity of starch, the Py-SNPs deformed in water to allow their hydrophobic pyrene labels to cluster toward the center of the SNPs to minimize pyrene-solvent contacts. This segregation of the hydrophobic pyrene labels led to a distinct core-shell structure for the Py-SNPs which was illustrated in TEM images acquired on films prepared with the Py-SNPs. In summary, this thesis has uncovered some unexpected properties of the SNPs. Their branched structure makes their interpenetration difficult in the

semi-dilute regime which forces them to contract. SNPs are thus deformable and their deformation can be probed quantitatively by using fluorescence and TEM.

Acknowledgements

First, I would like to thank my supervisor Dr. Jean Duhamel for accepting me as a M. Sc. student and supporting me through this project both academically and financially. This thesis would not have been completed without Professor Duhamel's help.

I would also like to thank Profs. Mario Gauthier and Xiaosong Wang for being members of my advisory committee, with special thanks to Prof. Juewen Liu for accepting to replace Prof. Mario Gauthier as one of the readers of my thesis. I am truly grateful to all the Duhamel and Gauthier group members who have always helped me to carry out my research, especially Shiva Farhangi, Lu Li, Bingqing Yang, Solmaz Pirouz, Mike Fowler, Remi Cassier, Dr. Toufic Aridi, Olivier Nguon, and Dr. Gregory Whitton. Thank you all for making my time in University of Waterloo fun and memorable.

Special thanks go to the Eco-Win team members, Prof. Scott Taylor, Ryan Amos, Joanne Fernandez, Duncan Li, Magda Karski, Imran khimji, Alexander Ip, Ziyi Sun, and Howard Tsi, and the scientists at EcoSynthetix, particularly Dr. Steven Bloembergen. I must also thank EcoSynthetix, NSERC, and the University of Waterloo for financial support.

Finally, I would like to express my gratitude to my parents and my sister for their support, sacrifice, and encouragements.

Dedication

To my loving parents

Kangliang Yi and Haiping Huang

And to my loving sister

Cong Yi

Table of Contents

List of Figures

List of Tables and Schemes

List of Abbreviations

DCM	dichloromethane
D_h	hydrodynamic diameter
DIAD	diisopropyl azodicarboxylate
DIC	diisopropylcarbodiimide
DLS	dynamic light scattering
DMF	*N*, *N*-dimethylformamide
DMSO	dimethyl sulfoxide
ECO	EcoSynthetix Inc.
FTIR	Fourier transform infrared spectroscopy
^{1}H NMR	proton nuclear magnetic resonance
HOBt	hydroxybenzotriazole
PBA	1-pyrenebutyryl group
PEG	poly (ethylene glycol)
PEO	poly (ethylene oxide)
PFQ	protective fluorescence quenching
PMe	1-pyrenemethyl group
Poly-Q	polymeric quencher
Py	Pyrene
SA	styrene-acrylate

SB	styrene-butadiene
SNPs	starch nanoparticles
SV	Stern-Volmer
THF	tetrahydrofuran
TPP	triphenylphosphine

Chapter 1

Introduction

1.1 Background

As the driving force of the modern industrialized world, petroleum is the most important source of energy and synthetic products used in our daily life. However, pressure arising from both the environment and the economy is gearing the world toward shifting its attention from old unsustainable sources of energy and raw chemicals to novel and renewable ones. In this regard, cellulose, starch, and their derivatives are good alternatives to replace petroleum and its products, because they are environmentally friendly, renewable, and cost effective.

As the second most abundant biomass material in nature, starch is produced by many plants such as corn, potato, cassava, and wheat where it is used to store energy. Although starch has been processed industrially for quite a long time, the structure of starch is poorly understood due to its complexity.[1] Figure 1.1 represents the current consensus on the multiscale structure of starch.[1] The coarsest scale is described by the granules (*a*) whose dimension ranges from 2 to 100 μm depending on the botanic origin of the starch. The second scale consists of growth rings (*b*) with diameters between 120 and 500 nm, which are constituted of small blocklets (*c*, 20-50 nm) with alternating lamellae made of crystalline amylopectin and amorphous amylase. The finest scale is represented by the basic building units of amylose (*h*) and amylopectin (*g*) (0.1-1 nm).[1]

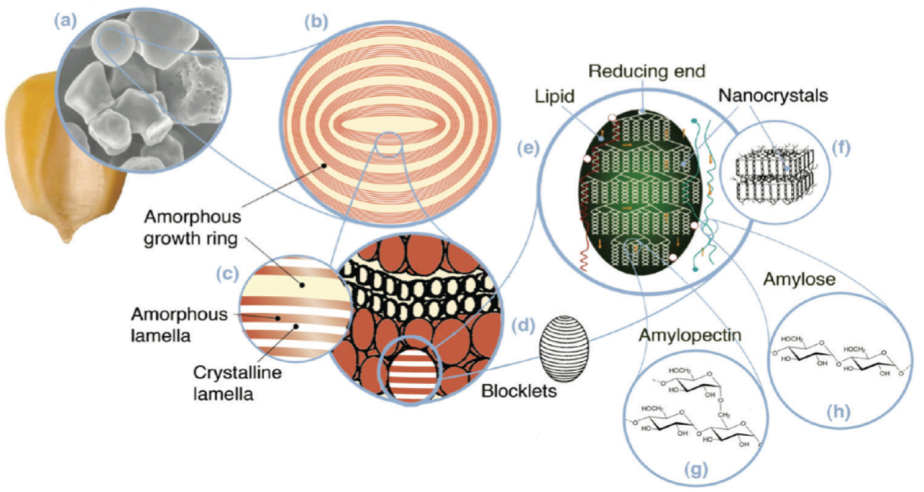

Figure 1.1. Multiscale structure of starch.[1]

The starch nanoparticles (SNPs) sold as EcoSphere® are produced by EcoSynthetix Inc, which is headquartered in Burlington, Ontario. Ever since it was founded in 1996, ECO has devoted itself to develop and commercialize biobased materials that combine good performance with environmentally-friendly impact. SNPs can be viewed as a relatively cheap and renewable type of carbohydrate-based biopolymer which is derived from starch. SNPs are being used in a number of applications that include paper coating. SNPs typically consist of mainly two types of glucosidic macromolecules, normally 72-82 w/w% linear-chain amylose and a complementary amount of branched amylopectin. The chemical structures of amylose and amylopectin are shown in Figure 1.2.[2]

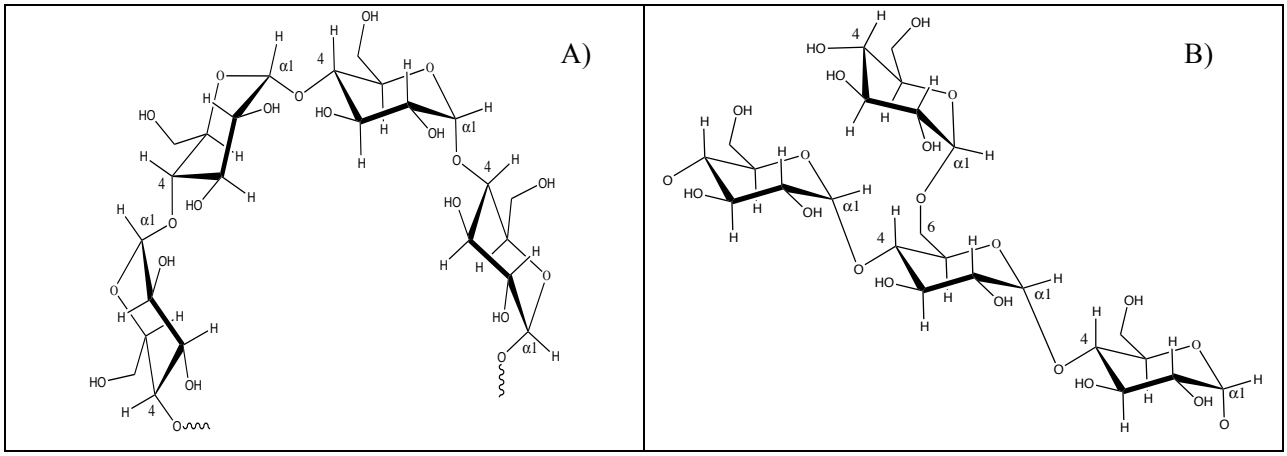

Figure 1.2. Chemical structures of A) amylose and B) amylopectin.[2]

As shown in Figure 1.2, amylose is a linear molecule constituted of glucose units linked by α-(1-4)-D-glycoside bonds. Amylose can adopt a helical conformation resulting in a stiff structure. Amylopectin on the other hand is highly branched with relatively short branches of 22 α-(1-4)-D-linked glucose units internally linked by α-(1-6)-D-glycoside bonds. Because of this interlinked network, amylopectin has a much higher molecular weight than amylose. Amylose molecules contain about 500-20,000 glucose units depending on the source, whereas each amylopectin molecule consists of up to two million glucose units, which are compacted into a relatively small volume.[3]

1.2 Structure and Properties of the SNPs prepared by EcoSynthetix

SNPs are prepared by crosslinking starch in a twin extruder. The starch can be obtained from a wide range of sources like potato, wheat, maize, rice, and cassava. The diameter of the SNPs varies depending on the crosslinking level. The amount of crosslinker and plasticizer (glycerol)

that are injected during extrusion can be adjusted to control the properties and crosslinking level of the nanoparticles.[4] The proposed structure of the crosslinked SNPs is shown in Figure 1.3. Crosslinking of starch in the extruder generates the SNPs which can be dispersed in water into a stable emulsion of swollen particles. These emulsions can shear-thin, a property that contributes to making SNPs an attractive binder in the paper coating process.[6]

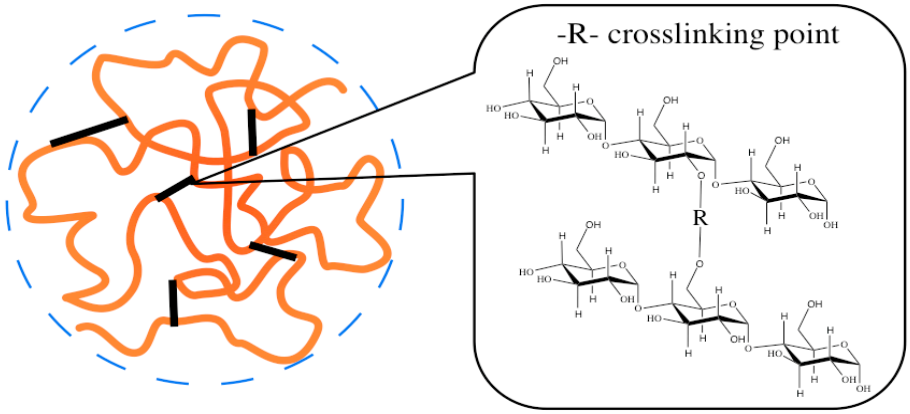

Figure 1.3. Proposed structure of SNPs.

1.3 Pyrene Fluorescence and Excimer Formation

1.3.1 Pyrene Fluorescence

Fluorescence describes a photophysical process whereby an excited electron in the singlet state goes back to the ground-state. During this process a photon with a well defined energy is emitted. The whole process is well-illustrated by the Jablonski diagram shown in Figure 1.4. Firstly, the dye in its lowest vibrational energy level of the electronic state S_0 absorbs a photon of energy $h\nu_{ex}$ and its corresponding wavelength is called the excitation wavelength λ_{ex}. This

process happens quickly within 10^{-15} s. After the absorption, the electron reaches one of the vibrational energy levels of the higher electronic states such as S_1 or S_2, depending on λ_{ex}. The excited dye then undergoes an internal conversion which brings the electron back to the lowest vibrational level of the S_1 electronic state. Internal conversion occurs over less than 10^{-12} s. The energy lost during this process leads to a red shift of the emission photon associated with an energy $h\nu_{em}$ when the electron returns to one of the vibrational levels of the ground-state. The loss in energy between the excitation and emission wavelength is referred to as Stokes' Shift. As one of the most important fluorescent dyes,[7,8] pyrene has long been used to probe the internal dynamics of macromolecules.[9,10-12]

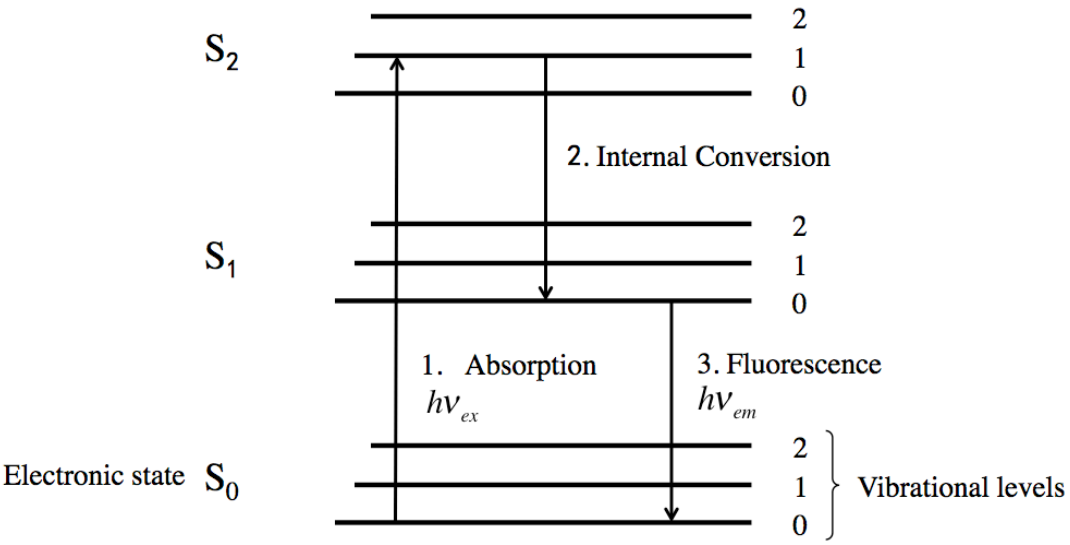

Figure 1.4. Jablonski diagram describing fluorescence.[7]

Pyrene is endowed with several impressive photophysical properties that make it unique. These properties are listed hereafter. Firstly, pyrene has a relatively high quantum yield (0.32 for pyrene in cyclohexane),[13] and a large molar absorbance coefficient, which make it possible to work at very low concentrations to avoid the inner filter effect.[16] Secondly, its long lifetime of 200-300 ns[14] in degassed organic solvents allows the experimentalist to study the slow chain dynamics of pyrene-labeled macromolecules.[8,10-13,17] Thirdly, pyrene can form an excimer by complexing with itself. This self-quenching mechanism means that pyrene acts as a fluorophore and a quencher, and as such, a single labeling step is required to attach the fluorophore and the quencher to the macromolecule. Lastly, pyrene has been the object of intense scientific scrutiny and its photophysical properties are well understood and they have been described in a number of reviews.[7-12] The chemical structure of pyrene is shown in Figure 1.5.

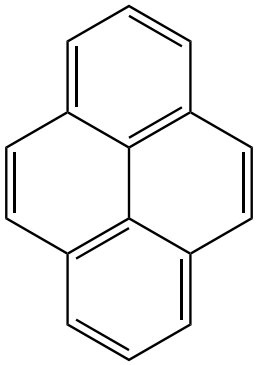

Figure 1.5. Chemical structure of pyrene.

1.3.2 Fluorescence Quenching

Fluorescence quenching represents any photophysical process leading to a decrease of the fluorescence intensity of a given fluorophore. There are many types of fluorescence quenching processes, such as dynamic quenching, static quenching resulting in the formation of a complex between the fluorophore and the quencher in the ground-state, energy or electron transfer and other reactions in the excited state that include excimer or exciplex formation.[12]

1.3.3 The I_E/I_M Ratio

The I_E/I_M ratio is one of the most basic, yet most useful features of pyrene fluorescence. The I_E/I_M ratio provides a qualitative measure of the amount of excimer formed relative to the monomer.[8] The ratio is calculated based on the steady-state fluorescence spectrum of the pyrene labeled polymers. The typical fluorescence spectrum of a pyrene-labeled macromolecule is shown in Figure 1.6.[8]

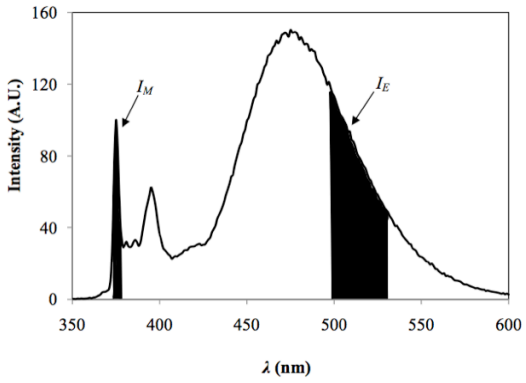

Figure 1.6. Steady-state fluorescence spectrum of hydrophobically modified cellulose labeled with pyrene (1 Py/26 glucose units, 0.026 g/L^{-1}) in water. Shaded areas represent the integration of the fluorescence spectrum to obtain a measure of I_M and I_E.[8]

The monomer fluorescence intensity (I_M) is integrated over the 375-380 nm wavelength range, while the excimer fluorescence is broad and centered at around 480 nm and its intensity (I_E) is obtained by integrating the fluorescence spectrum between 500-530 nm.[8] The I_E/I_M ratio is obtained by dividing I_E by I_M. The internal chain dynamic of polymer can be characterized by the I_E/I_M ratio, since it depends on the diffusive motion of the chain and also the local pyrene concentration. Although the I_E/I_M ratio provides us with some useful information about the properties of a pyrene-labeled macromolecule, it cannot distinguish between an excimer that is formed by the diffusive encounter between an excited and a ground-state pyrene and the direct excitation of aggregates of ground-state pyrenes. The origin of the pyrene excimer can be determined by conducting a time-resolved fluorescence experiment. As shown in Figure 1.7, the sample is excited at 344 nm and the monomer and excimer decays are acquired at 375 nm and 510 nm, respectively. By coupling the kinetics of excimer formation in the monomer and excimer decays, more accurate information about the parameters describing the kinetics of excimer formation and the nature of the pyrene species in solution, whether they are isolated and do not form excimer or form excimer by diffusion or direct excitation of a pyrene aggregate. The quality of the decays is determined by the residuals and autocorrelation function of the residuals as shown in Figure 1.7. The random distribution of the signal around zero (for both residual and autocorrelation function) indicates a good fit of the decays.

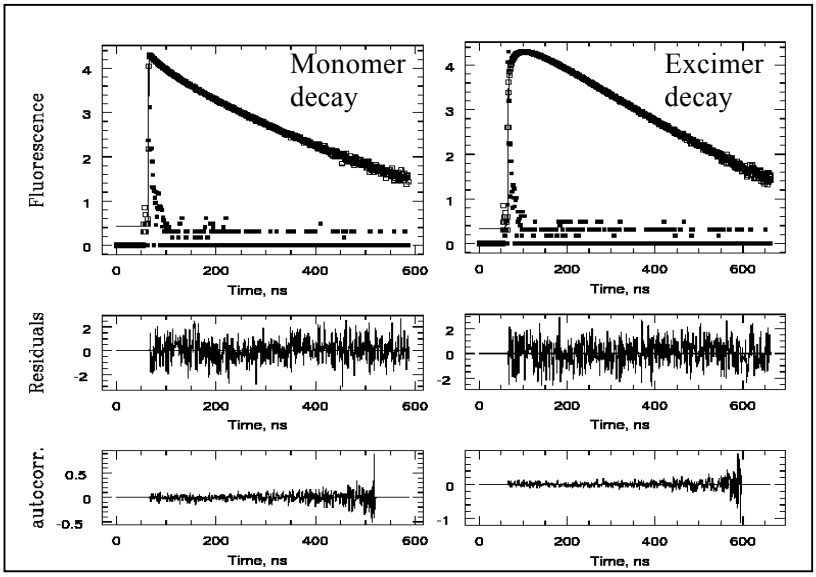

Figure 1.7. Monomer and excimer decays of terminally substituted polystyrene with pyrene in THF.[15]

Cuniberti and Perico suggested that the I_E/I_M ratio for a pyrene-labeled polymer is given by Equation 1.1.[15]

$$\frac{I_E}{I_M} = \kappa \frac{\varphi_E^0}{\varphi_M^0} \tau_M k_1 [Py]_{loc} \qquad 1.1$$

In Equation 1.1, κ is a constant that depends on the geometry and sensitivity of the instrument used, φ_M^0 and φ_E^0 are the fluorescence quantum yields of the pyrene monomer and excimer, respectively, τ_M stands for the natural lifetime of the pyrene monomer, and k_1 represent the bimolecular encounter rate constant which for molecular pyrene in solution would equal $2RT/(3\eta)$ with R, T, and η being, respectively, the ideal gas constant, the absolute temperature

in K, and the viscosity of the solvent at T. Finally, $[Py]_{loc}$ represents the local concentration of pyrene units attached to the macromolecule. For a certain system $\varkappa$, ϕ^0_E, ϕ^0_M are constants. Combining these constants into K, Equation 1.1 can be simplified into Equation 1.2. According to Equation 1.2, the I_E/I_M ratio is proportional to the product $k_1[Py]_{loc}$. Since k_1 is the rate constant for the diffusive encounters between two pyrene labels covalently attached onto a macromolecule, the proportionality that exists between the I_E/I_M ratio and k_1 implies that I_E/I_M is a measure of the rate constant of excimer formation.

$$\frac{I_E}{I_M} = Kk_1[Py]_{loc} \qquad 1.2$$

One of the major applications of SNPs is in the paper industry where they work as binder for paper coating to smooth the rough surface of untreated paper generated by the cellulose fibers. The thin binder layer provides a smooth surface to print and write. Hence it becomes quite important to characterize how SNPs behave when they are dispersed in the binder solution. The proper intermolecular interactions between dispersed SNPs result in a smooth, jam-free coating process. In this study, pyrene is covalently attached onto SNPs and the I_E/I_M ratio will be employed to obtain dynamic and structural information about the SNPs in both solution or in the bulk. The process of pyrene excimer formation in a pyrene-labeled SNP is described in Scheme 1.1. A ground-state pyrene can absorb a UV photon at 340 nm, yielding an excited pyrene monomer that can either fluoresce with a rate constant τ_M^{-1} where τ_M is the pyrene monomer lifetime or encounter a ground-state pyrene to form an excimer. In Scheme 1.1, the time-

dependent rate constant for excimer formation is described by $f(t)$. Similarly, the excimer can also fluoresce with a rate constant τ_{EO}^{-1} where τ_{EO} is the excimer lifetime or dissociate with the rate constant k_{-1}. In most applications, k_{-1} is small compared to $1/\tau_{EO}$ so that it can be neglected as long as the solution temperature is smaller than 35 °C.[11]

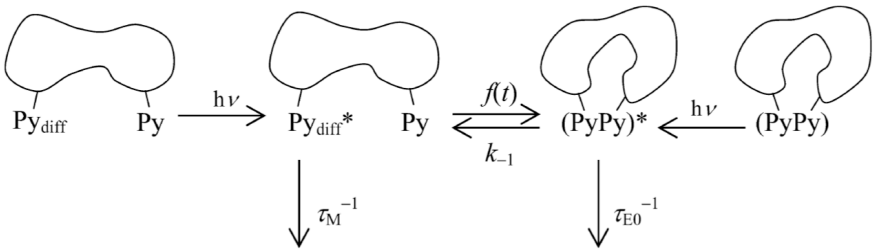

Scheme 1.1. Excimer formation between pyrenes covalently attached to a macromolecule.

1.4 Outline of the Thesis

This thesis is organized in the following manner. Chapter 2 presents the three attempts that were made to label the SNPs with pyrene. The first method involves the nucleophilic attack of 1-pyrenemethylenechloride by alkoxides produced by the deprotonation of the starch hydroxyls. The second method was introduced to avoid the degradation of the SNPs induced by sodium hydride used in the first method. NaH was replaced by the milder base dimethylaminopyridine (DMAP). Although the second method did not degrade the SNPs, the resulting pyrene labeling level was too small. Consequently, a third synthetic procedure was developed where 1-pyrenebutanoic acid was coupled to the starch hydroxyls with diisopropylcarbodiimide (DIC) and DMAP as the base. Method 3 was selected to conduct the labeling reaction because the

SNPs did not degrade and it also yielded measurable pyrene contents ranging between 0.5 and 5 mol%. Chapter 3 describes the two types of PEG-based quenchers that were synthesized to carry out the quenching experiments. The first one, a pyridinium terminated Me-PEG was quickly abandoned as it was found to decompose over time. The second polymeric quencher terminated with a nitro group was applied to quench the pyrene-labeled SNPs (Py-SNPs) prepared in Chapter 2. The solution behavior of the Py-SNPs was investigated in Chapter 4. The chain dynamics and morphology of the SNPs were characterized by steady-state and time-resolved fluorescence and transmission electron microscopy. Finally, Chapter 5 summarizes the main results of the previous chapters and suggests some future work.

Chapter 2

Synthesis and Characterization of Pyrene-Labeled Starch Nanoparticles

2.1 Experimental Procedures

2.1.1 Chemicals

The solvents dimethyl sulfoxide (DMSO) (reagent grade, 98.0%, Caledon), dimethylformamide (anhydrous, 99.8%, Sigma-Aldrich), acetone (HPLC grade, Caledon), tetrahydrofuran (THF ≥99.9%, Caledon), and methanol (HPLC, ≥99%, Caledon) were used as received. Sodium hydride (NaH) (60% dispersion in mineral oil), 4-(dimetylamino) pyridine (≥99%), N,N'-diisopropylcarbodiimide (DIC) (≥98.0%), 1-pyrenemethanol (98%), and 1-pyrenebutyric acid (97%) were purchased from Sigma-Aldrich and used as received.

2.1.2 Instrumentation

2.1.2.1 Nuclear Magnetic Resonance (NMR)

The ^{1}H NMR spectra of the SNPs were obtained with a Bruker 300 MHz high resolution NMR spectrometer. Deuterated DMSO (99.9 atom % D, Sigma-Aldrich) was used as the solvent. The concentration used to acquire the ^{1}H NMR spectra of the SNPs was at least 30 mg/mL to ensure a sufficient signal-to-noise ratio.

2.1.2.2 Dynamic Light Scattering (DLS)

The distribution of hydrodynamic diameters (D_h) of the SNPs was obtained with a Malvern Zetasizer Nano S90. SNP solutions were prepared with DMSO or Mili-Q water. The SNP concentrations used to acquire the autocorrelation functions of the scattering intensity whose analysis yielded D_h were greater than 0.1 w/w%. The DLS experiments were conducted at 25 °C.

2.1.2.3 Steady-State Fluorescence

The steady-state fluorescence spectra of the pyrene-labeled SNPs (Py-SNPs) were obtained with a Photon Technology International (PTI) LS-100 steady-state fluorometer, which was equipped with an Ushio UXL-75Xe Xenon arc lamp and a PTI 814 photomultiplier detection system. A quartz cuvette with a 10 mm path length was used to measure the fluorescence spectra. Samples were excited at 346 nm and emission was monitored form 350 to 600 nm. The concentration of Py-SNP solutions used in these measurements corresponded to a pyrene concentration of 2.5 μM. For a given Py(x)-SNP(y) sample representing a Py-SNP containing x = 5 mol% of pyrene obtained by labeling an SNP extruded with y = 0 w/w% crosslinking agent, a 2.5 μM concentration of pyrene represents a massic concentration of 8.4 mg/L. Such low SNP concentrations ensure that no intermolecular excimer formation is being observed. The Py-SNP solutions in water or DMSO were not degassed.

2.1.2.4 Time-Resolved Fluorescence Measurements

The fluorescence decays of the pyrene monomer and excimer of the Py-SNP solutions were acquired on an IBH time-resolved fluorometer equipped with a nanoLED light source. The solutions were excited at 346 nm and the monomer and excimer emission was monitored at 375 nm and 510 nm, respectively. The fluorescence decays were acquired with a 370 nm and 495 nm cut-off filter to prevent stray light scattering from reaching the detector, respectively. A Ludox solution was used to acquire the instrument response function which was applied to the fluorescence decay analysis. The solutions were prepared with a pyrene concentration of 2.5 μM.

2.1.2.5 Ultraviolet-Visible Absorption Spectroscopy

The absorption spectra were acquired on a UV-Vis spectrophotometer (Model CARY-100, Welltech Enterprises, INC., Maryland, USA).

2.2 Characterization of the SNPs

2.2.1 Purification of the SNPs

This step was necessary to free the SNPs from small unreacted molecules such as plasticizer or crosslinking agent left in the samples after the extrusion process. The SNPs (10 w/w%) were dispersed in DMSO at 50 °C for 24 hours with continuous stirring. The dispersion was then precipitated dropwise into cold methanol which had been placed in a beaker equipped with a stir bar. After stirring for an hour, the precipitate was allowed to settle at the bottom of the beaker. The mixture was passed through a glass filter. After the filtration was complete, the product was washed with acetone four times. The SNPs were collected and dried in a vacuum oven overnight. The purified SNPs had a color that ranged from white to light brown depending on the amount of crosslinker used in their synthesis, the SNPs prepared with more crosslinker showing a darker brown color. The successful removal of the plasticizer and crosslinking agent was confirmed by visual inspection of the ^{1}H NMR spectrum.

2.2.2 ^{1}H NMR Assignments of the SNP Protons

The chemical shifts and assignment of the peaks found in the ^{1}H NMR spectrum of the purified and unpurified SNPs are shown in Figure 2.1. The proton signal from the plasticizer (glycerol), crosslinking agent (glyoxal), water, and solvent were assigned first. The peak at 2.5 ppm belongs

to the solvent DMSO. The peak at 3.1 - 3.5 ppm is from water. The jagged contour of the water peak suggests that there are other chemicals in the sample whose ^{1}H NMR signal overlaps the water peak. These peaks disappeared after purification of the SNPs as the envelop of the water peak showed a smoother contour. The peaks between 4.1 and 4.6 ppm are due to unreacted glyoxal and glycerol. The peaks between 6.2 and 6.7 ppm are due to other forms of glyoxal. After purification, the signal from glycerol and glyoxal was no longer visible and the ^{1}H NMR spectrum of the purified SNPs was the same as that of starch.[19]

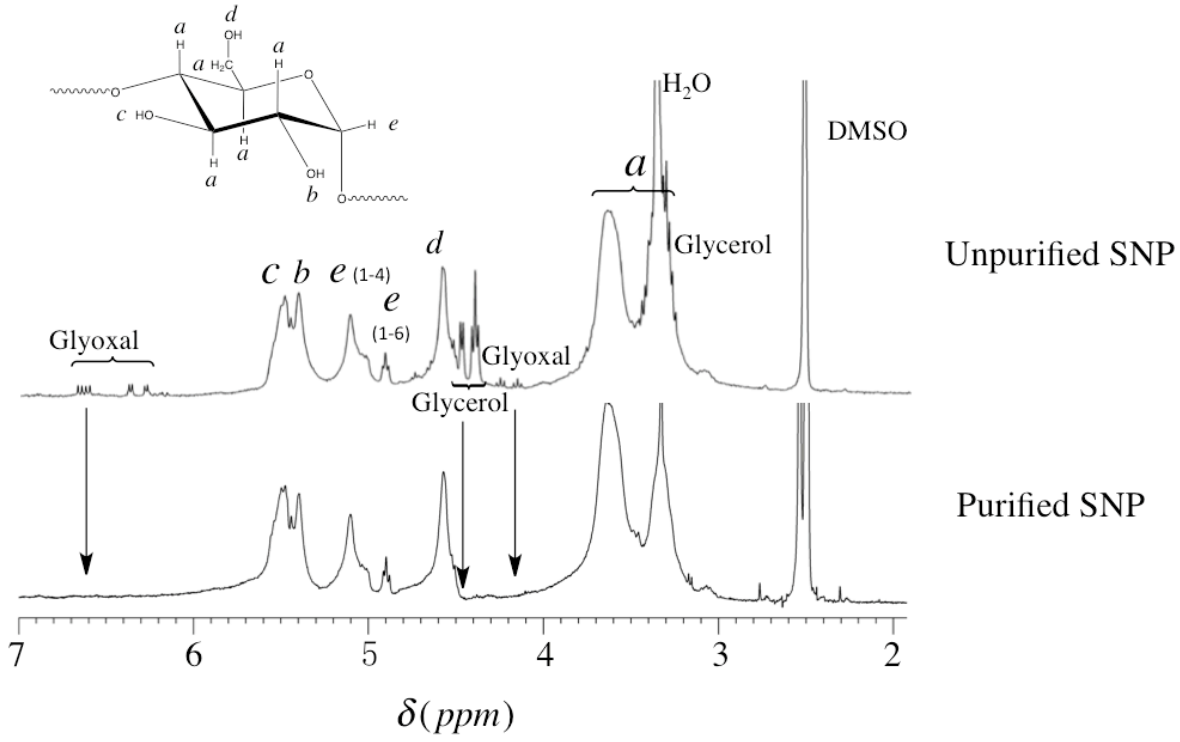

Figure 2.1 ^{1}H NMR assignment of the purified and unpurified SNPs.

The assignment of the different peaks found in the ^{1}H NMR spectrum of the SNPs is provided in Table 2.1 with the chemical shift corresponding to the protons of starch, plasticizer (glycerol), and crosslinker (glyoxal).

Table 2.1 Chemical shifts and assignment of the protons in the ^{1}H NMR spectrum of the unpurified SNPs.

Chemical Shift (ppm)	Assignments
6.2-6.7	OH (glyoxal)
5.5	OH-c (SNP)
5.4	OH-b (SNP)
5.1	OH-e (SNP)
4.9	CH-f (SNP)
4.6	OH-d (SNP)
4.4-4.6	OH (glycerol)
4.1-4.3	CH (glyoxal)
3.1-3.9	CH-a (SNP+glycerol)

2.3 Synthesis and Characterization of the Py-SNPs

2.3.1 Synthesis of the Py-SNPs

Three different methods were attempted to label the SNPs with pyrene. The first method used starch partially deprotonated by NaH to generate alkoxides along the starch backbone to induce the nucleophilic substitution of an activated derivative of 1-pyrenemethanol. To this end, tosylation of 1-pyrenemethanol with *p*-toluenesulfonic acid was attempted but found to be

unsuccessful probably due to steric hindrance. The chlorination of 1-pyrenemethanol with thionyl chloride was found to be efficient. For this reaction, 1-pyrenemethanol (1 g, 4.4 mmol) purified by crystallization from methanol was dissolved into 10 mL of freshly distilled chloroform in a round bottom flask, which was flamed 3 times beforehand under vacuum in order to remove residual moisture before being kept under a positive nitrogen atmosphere. Thionyl chloride (1 g, 8.4 mmol) was added dropwise with constant stirring. The mixture was allowed to react overnight at room temperature (RT) in the dark under nitrogen atmosphere. After evaporation of the solvent, 1-pyrenemethyl chloride (Py-CH_2-Cl) was recovered as a green powder at the bottom of the flask (0.91 g, yield =84.4%).[20]

The purified SNPs (1.6 g, 10 mmol in terms of glucose units) were dispersed in 20 mL DMSO that had been freshly distilled under reduced pressure. The SNP dispersion was kept at 50 °C in an oil bath. Py-CH_2-Cl (1.25 g, 5.6 mmol) was dissolved in 2 mL of DMSO before being added to the SNP dispersion. The mixture was stirred for 5 hours in order to allow Py-CH_2-Cl to penetrate the interior of the SNPs. NaH (0.4 g, 10 mmol) was then added to the mixture. After 5 hours of reaction, the green solution turned into a dark-brown colored gel. DMSO (10 mL) was added to the gel and the crude product was precipitated in 400 mL of cold methanol. The precipitation step was repeated 5 times yielding 0.42 g (26.3%) of grey-white product.[20]

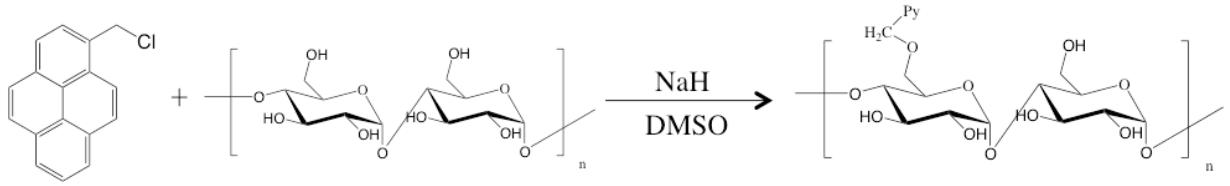

Scheme 2.1. First synthetic route for labeling the SNPs with 1-pyrenemethanol.

The first synthetic route turned out to be unsuccessful. Sodium hydride was found to be too strong a base, which degraded the SNPs at NaH concentrations higher than 15 mg/mL. The effect of NaH concentration on the SNPs is illustrated in Figure 2.2. The solution turned darker with increasing NaH concentration indicating that NaH reacted with the SNPs.

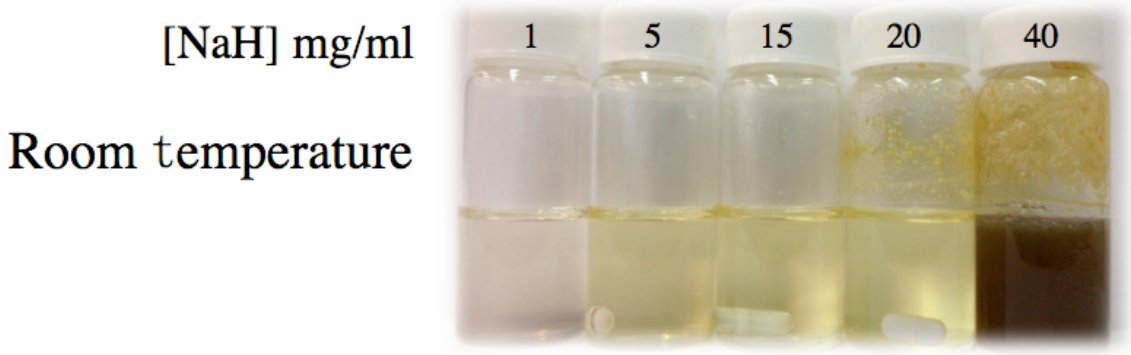

Figure 2.2. Effect of NaH concentration on the SNPs.

In fact, the SNPs started to precipitate for the NaH concentration larger than 20 mg/mL. At 40 mg/mL, the whole solution turned black. In these experiments, the SNP concentration equaled 40 mg/mL and the mixture was left to react for 8 hours. The particle sizes were checked by DLS and the hydrodynamic diameters shown in Table 2.2 confirmed the decomposition of the particles induced by NaH.

Table 2.2. Reaction conditions and corresponding D_h of SNPs after reaction.

Samples	Solvent	[NaH] mg/mL	[SNP] mg/mL	Time (hr)	D_h (nm) before	D_h (nm) after
SNP0	DMSO	40	40	8	42	10
SNP0	DMSO	20	40	8	42	2.7
SNP0	DMSO	15	40	8	42	polydispersed
SNP0	DMSO	5	40	8	42	10
SNP0	DMSO	1	40	8	42	41

In the second procedure used to label the SNPs with pyrene and referred to as Method 2, 1-pyrenebutyric acid (PBA) was selected as the pyrene derivative and DMAP as the base. The purified SNPs (1.0 g, 6.2 mmol in terms of glucose units) were freeze-dried before being dispersed in 40 mL DMSO to which PBA (0.2 g, 0.68 mmol) and DMAP (0.4 g, 3.3 mmol) were added. The dispersion was stirred for 1 hour. The reaction was conducted at different temperatures (room temperature, 50 °C, and 100 °C) for 24 hours under nitrogen atmosphere and in the dark. The synthetic route for Method 2 is shown in Scheme 2.2. The crude product was precipitated four times in 400 mL of cold tetrahydrofuran (THF) yielding 0.51 g (51%) of white product.[21]

Table 2.3. Reaction conditions for Method 2.

Samples	[py] mmol/L	[DMAP] mmol/L	[glucose] mmol/L	T°C	Time hr	D_h(nm) before	D_h(nm) after	Mol% py
SNP6	17	82	154	25	8	27	25	unavailable
SNP6	17	82	154	50	8	27	24	unavailable
SNP6	17	82	154	100	8	27	9	unavailable

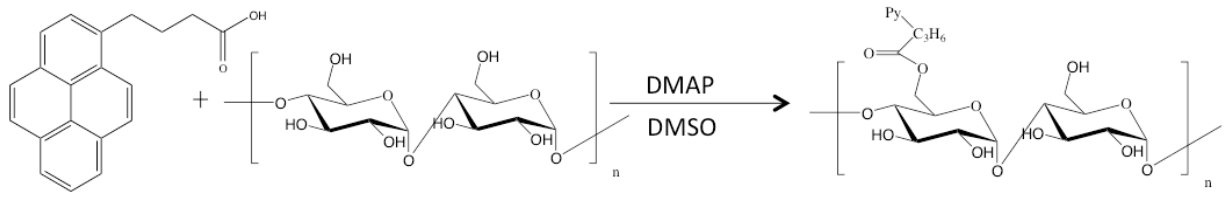

Scheme 2.2. Labeling of the SNPs with pyrene according to Method 2.

The particles were found to degrade when the labeling reaction was conducted at 100 °C. Although the SNPs retained their size when the reaction was carried out at 25 °C and 50 °C, the resulting level of pyrene labeling was really low as hardly any absorption could be detected at 346 nm where pyrene absorbs. In order to increase the pyrene labeling level, a third synthetic route referred to as Method 3 was investigated.

In Method 3, diisopropylcarbodiimide (DIC) was used as a coupling agent and a 1:3 mixture of dimethylformamide (DMF) and DMSO was used as the solvent. Because the melting point of DMSO is 19 °C, the addition of DMF prevented the solution from freezing at 0 °C, and the amount of DMF added was low enough to ensure that the SNPs were well-dispersed in the solvent mixture. SNP0 and SNP5 where the numbers 0 and 5 correspond to the w/w% percentage of crosslinking agent used during the extrusion were purified and freeze-dried before use. The SNPs (0.97 g, 6 mmol in terms of glucose units) were dispersed in 40 mL of the 3:1 mixture of DMSO (30 mL) and DMF (10 mL), which was followed by the addition of PBA (0.18 g, 0.63 mmol) and DMAP (0.17 g, 1.4 mmol). The amounts of PBA and DMAP could be adjusted to obtain the desired pyrene content. The mixture was put in an ice bath (0 °C) and DIC (0.55 g, 4.4

mmol) was added dropwise over a 30 minute period. The solution was then brought back to room temperature and was left stirring for 48 hours under nitrogen atmosphere and kept in the dark. The reaction scheme for Method 3 is shown in Scheme 2.3. The crude product was precipitated four times into 400 mL of cold tetrahydrofuran (THF).[21,22]

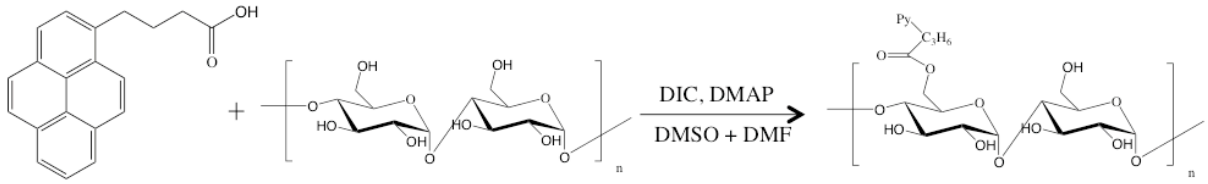

Scheme 2.3. Labeling of the SNPs with pyrene according to Method 3.

2.3.2 Characterization of the Pyrene-Labeled SNPs

Since Method 3 yielded a decent level of pyrene labeling without inducing SNP degradation, the majority of results presented in this thesis were obtained from experiments conducted on PBA-SNPs generated according to Method 3. The condition reactions used to synthesize the PBA-SNPs according to Method 3 are listed in Table 2.4.

Table 2.4. Reaction conditions according to Method 3

Sample	[Py] mmol/L	[DMAP] mmol/L	[glucose] mmol/L	[DIC] mmol/L	Time (hr)	D_h(nm) before	D_h(nm) after	x_{py} mol%py
SNP0	20	34.8	149	30	48	32	29	0.05%
SNP5	20	34.8	149	30	48	14	15	0.04%
SNP0	74	15	149	110	48	31	34	5%
SNP5	74	15	149	110	48	13	15	5%

The products of these reactions were characterized by ^{1}H NMR, UV-Vis spectroscopy, and steady-state and time-resolved fluorescence. The results of these experiments are discussed hereafter.

2.3.2.1 ^{1}H NMR Spectroscopy

The ^{1}H NMR spectrum of the SNPs labeled with 1-pyrenebutyric acid (PBA-SNP) is shown in the top panel of Figure 2.3. The ^{1}H NMR spectrum shown in the middle panel of Figure 2.3 was obtained for the purified SNPs, and the spectrum in the bottom panel is that of PBA. After pyrene labeling, new peaks appeared in the ^{1}H NMR spectrum of the SNPs. The proton signal at 2.0 ppm belongs to the β-methylene protons of PBA, and the peaks between 7.80 and 8.40 ppm correspond to the aromatic protons of pyrene.

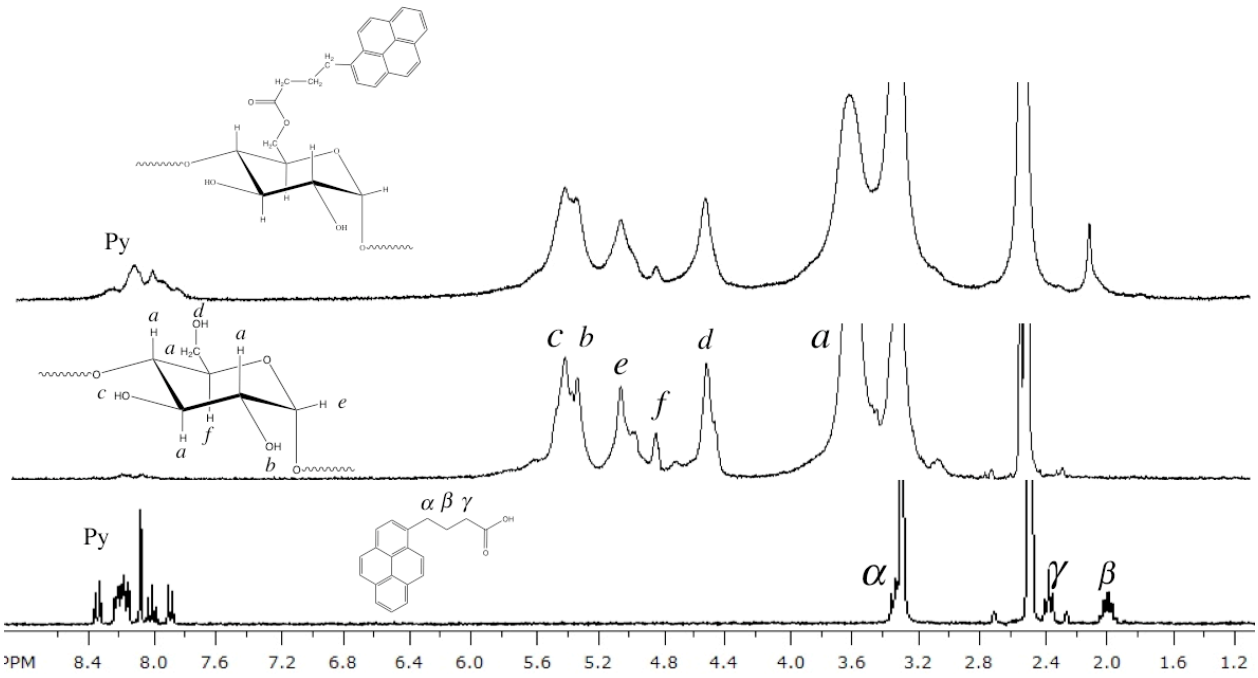

Figure 2.3. [1]H NMR spectra of (top) PBA(5)-SNP0, (middle) SNP0, and (bottom) PBA.

The [1]H NMR spectrum of PBA shows the signal of the methylene protons α, β, and γ found at 3.3, 2.0, and 2.4 ppm, respectively. Only the β-methylene proton of PBA appeared in the spectrum of SNP-PBA, since the [1]H NMR signal of the α-proton of PBA overlaps the signal of the a-proton of the SNP (see Table 2.1). The disappearance of the γ-proton of PBA from the [1]H NMR spectrum might be attributed to a downfield shift bringing it under the water signal at 2.5 ppm.

2.3.2.2 Dynamic Light Scattering

To ensure that the nanoparticles did not decompose after the labeling reaction, the hydrodynamic diameter (D_h) was measured by dynamic light scattering (DLS) both before and after labeling the SNPs with PBA. All D_h measurements were conducted by acquiring the autocorrelation function of the light scattering signal over 5 minutes. The autocorrelation function was fitted with a sum of exponentials to yield a histogram based on the number percentage of the D_h values representative of the SNP population. Each DLS experiment was repeated four times yielding four autocorrelation functions and thus four number-averaged D_h values. Figure 2.4 shows the D_h histograms for the unlabeled SNP0 and SNP5 samples as well as the corresponding histograms obtained for the SNPs labeled with PBA according to the third synthetic route given in Scheme 2.3. The SNP0, PBA(5)-SNP0, SNP5, and PBA(5)-SNP5 samples had an average D_h value of 45.0 ± 6.4 nm, 49.6 ± 9.0 nm, 12.2 ± 1.6 nm, and 16.8 ± 1.3 nm, respectively. It is important to note that D_h for SNP0 is larger than the value of 31 nm reported in Table 2.4 because these samples were obtained through two different extrusion processes. Labeling of the SNPs with PBA seems to yield slightly larger SNPs, possibly due to the better solubility of the Py-SNPs in DMSO that resulted in the swelling of the particles.

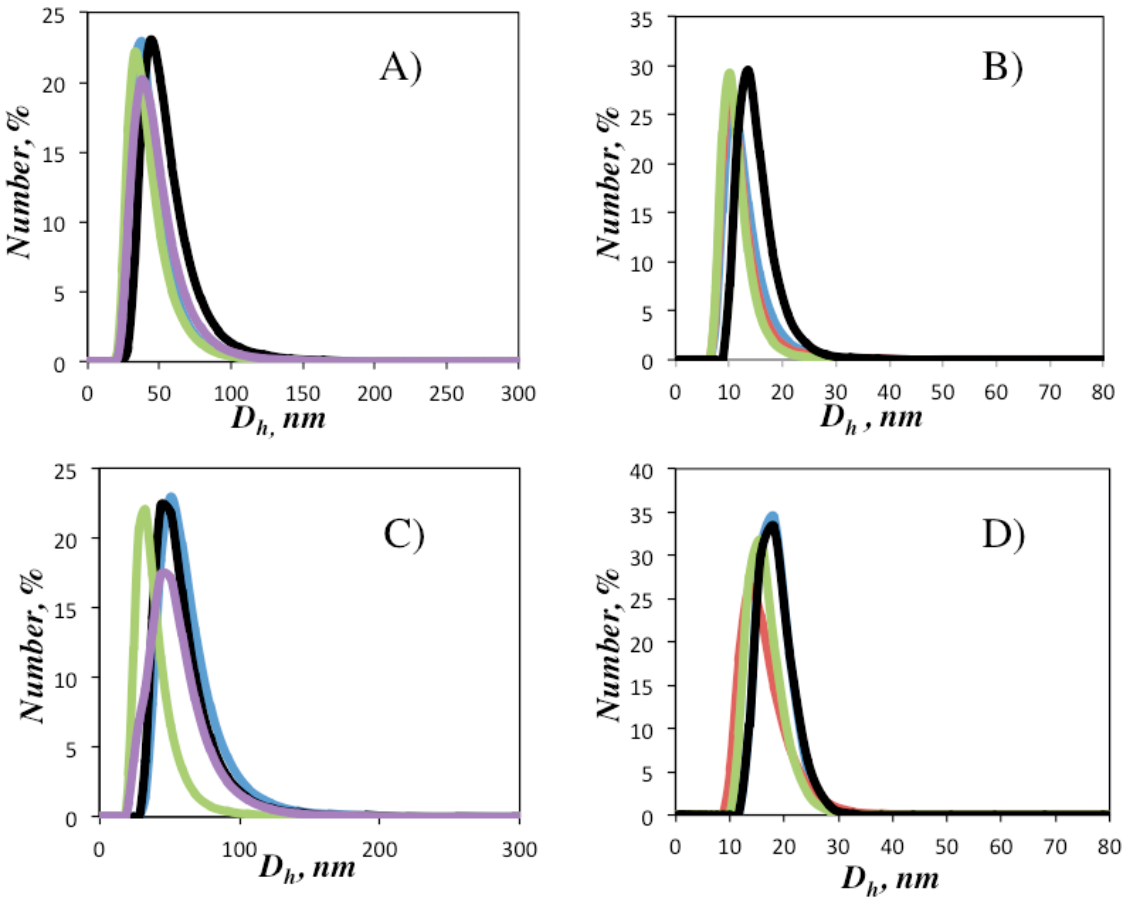

Figure 2.4. Histograms of D_h values obtained for the particles of two unlabeled and PBA-labeled SNPs. A) SNP0 (D_h =45.0 ± 6.1 nm); B) PBA(5)-SNP0 (D_h =49.6 ± 9.0 nm); C) SNP5 (D_h =12.2 ± 1.6 nm); D) PBA(5)-SNP5 (D_h =16.8 ± 1.3 nm).

2.3.2.3 Ultraviolet-Visible Absorption Spectroscopy

The UV-Vis absorption spectrum of a 0.17 g/L PBA(5)-SNP0 solution in DMSO is shown in Figure 2.5. The spectrum was compared to that of a 25 μM DMSO solution of PBA, and these two spectra overlapped perfectly, thus confirming that the labeling reaction did not affect the absorption of PBA and that UV-Vis absorption could be applied to determine the pyrene content,

λ_{py}, of the Py-SNPs. This was done with Equation 2.1 where λ_{py} is the pyrene content of a given Py-SNP expressed in terms of moles of pyrene per gram of SNP.

$$\lambda_{PY} = \frac{Abs}{\varepsilon_{py} \times [SNP]} \qquad 2.1$$

In Equation 2.1, [Py-SNP] is the mass concentration of the Py-SNP sample, and ε_{py} is the molar absorbance coefficient of PBA in DMSO found to equal 41400 $L \cdot mol^{-1} \cdot cm^{-1}$ at 346 nm in DMSO. The pyrene content λ_{py} could then be used to determine the mole fraction of glucose units that were labeled with PBA thanks to Equation 2.2.

$$x = \frac{\lambda_{py} M_{glu}}{1 + \lambda_{py}(M_{glu} - M_{py+glu})} \qquad 2.2$$

In Equation 2.2, x represents the molar fraction of glucose units that are labeled with a pyrene moiety. $M_{Py\text{-}Glu}$ and M_{Glu} represent the molar masses of the PBA-labeled and unlabeled glucose units equal to 432 and 162 $g \cdot mol^{-1}$, respectively.·

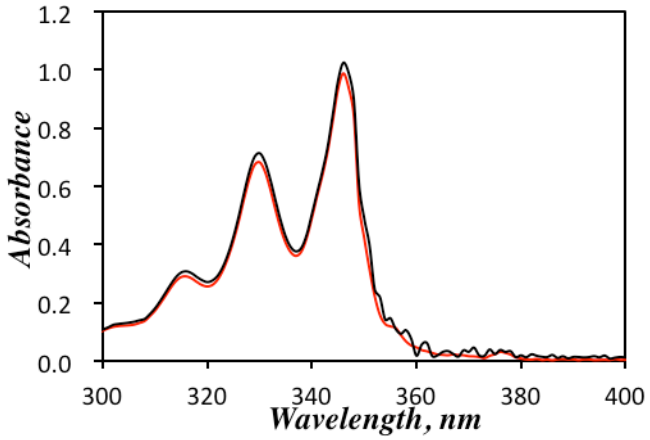

Figure 2.5. Absorption spectrum of 0.17 g/L Py(2.5)-SNP0 and 25 μM PBA solutions in DMSO.

2.3.2.4 Steady-State and Time-Resolved Fluorescence

Steady-state and time-resolved fluorescence measurements were applied to study the Py-SNPs. The steady-state fluorescence spectrum of the Py(5)-SNP0 sample is shown in Figure 2.6.

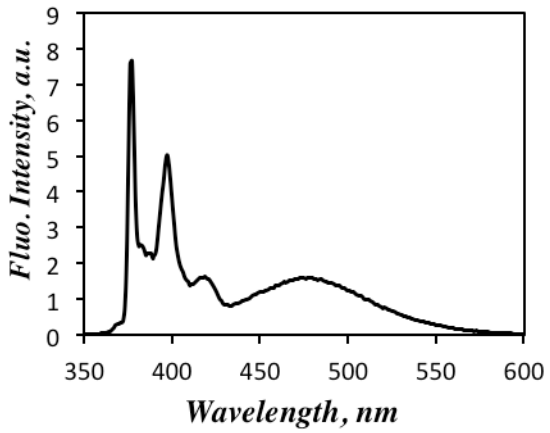

Figure 2.6. Fluorescence spectrum of a 8.5 mg/L solution of Py(5)-SNP0 sample in DMSO; λ_{ex} = 346 nm.

The steady-state fluorescence spectrum of the Py(5)-SNP0 solution showed the characteristic peaks of the pyrene monomer between 370 and 400 nm, and a broad structureless band corresponding to the pyrene excimer between 450 and 550 nm. For the fluorescence decay measurements, the Py-SNPs solution was excited at 346 nm and the emission was monitored at 375 nm and 510 nm for the pyrene monomer and excimer, respectively. Coupling of the kinetics of the monomer self-quenching and excimer formation allows for global analysis of the monomer and excimer decays, which improves the accuracy of the kinetic parameters that describe pyrene excimer formation. While the intensity of the monomer fluorescence decay in Figure 2.7A decreases continuously, the excimer intensity in Figure 2.7B shows a rise time reflecting the time taken by an excited and a ground-state pyrene to diffuse toward each other, encounter, and form an excimer.

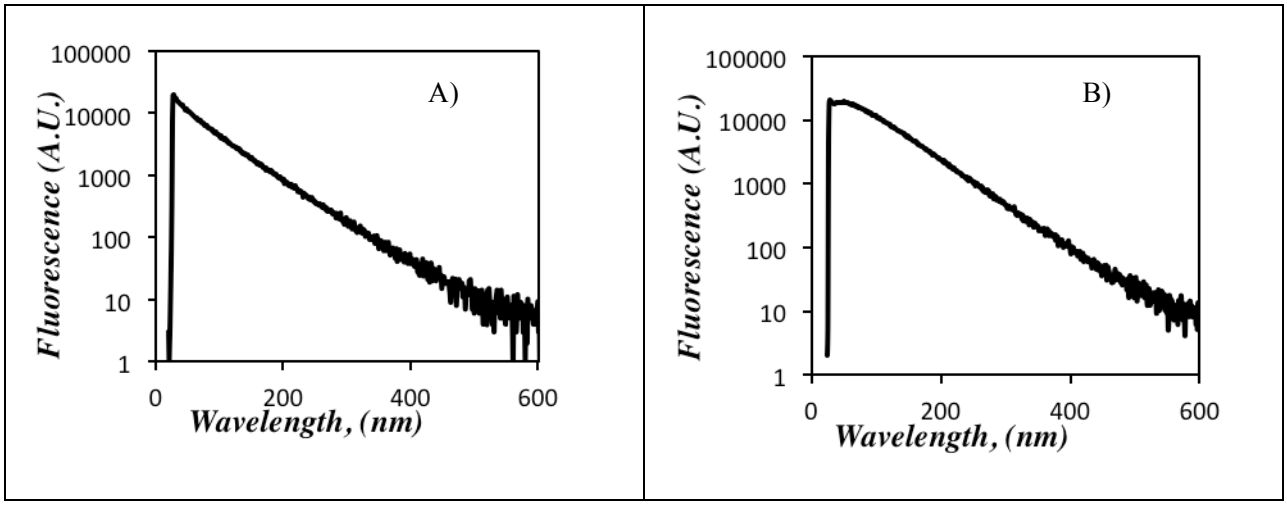

Figure 2.7. Fluorescence decays of a 8.5 mg/L Py(5)-SNP0 solution in DMSO. A) pyrene monomer (λ_{ex} =346 nm, λ_{em} =375 nm); B) pyrene excimer (λ_{ex} =346 nm, λ_{em} =510 nm).

If all excimer was produced by diffusive encounters between pyrene monomers, no excimer would be observed at the time where the solution was irradiated. This is not the case as can be seen in Figure 2.7 B), indicating that ground-state pyrene dimers exist in the solution and that they generate excimer instantaneously upon direct excitation.

The fact that the Py-SNPs form excimer at an overall pyrene concentration in DMSO of 2.5 μM is a good indication that the pyrenes are covalently attached to the SNPs. At such a low concentration, two free pyrenes would not be able to diffuse and encounter to form an excimer during the time (< 1 μs) pyrene remains in the excited state.

2.4 Conclusions

This chapter established a successful synthetic procedure to covalently label SNPs with 1-pyrenebutyric acid. The procedure preserved the structural integrity of the SNPs as demonstrated by comparing the D_h value of the particles before and after pyrene labeling. The photophysical properties of pyrene appeared to be unaffected by the labeling reaction as found from the visual inspection of the UV-Vis absorption and steady-state fluorescence spectra. The Py-SNPs can now be utilized to conduct fluorescence quenching experiments to investigate their ability to form excimer under different conditions.

Chapter 3

Synthesis and Characterization of a Polymeric Quencher

3.1 Introduction

Fluorescence quenching is a probing technique that is wildly used in both chemical and biochemical research. Fluorescence quenching can be static or collisional and both types of quenching require that the fluorophore and quencher interact with each other at the molecular level. In these experiments, the fluorescence of pyrene covalently attached to the starch nanoparticles (SNPs) according to the procedure referred to as Method 2 in Chapter 2 is monitored as a function of quencher concentration to characterize the accessibility of the fluorophore to the quencher.[16]

To this end, polymeric quenchers (Poly-Qs) with different molecular weights were prepared to probe the accessibility of the SNPs to Poly-Qs. The polymer selected in this study to prepare the Poly-Qs was Me-PEG-OH, a poly(ethylene glycol) chain terminated at one end with a methyl group and with a hydroxyl group at the other end. The quenching rate was expected to depend on the size of Poly-Q as a larger chain might not be able to access and quench the pyrene labels inside the Py-SNPs as easily as a shorter chain does. The synthesis and characterization of Poly-Q is described hereafter.

3.2 Experimental Procedures

3.2.1 Chemicals

The solvents chloroform (HPLC grade, ≥ 99.9%, Aldrich), dichloromethane (DCM, ≥ 99.9%, Aldrich), dimethyl sulfoxide (DMSO, 99.9 atom% D, Cambridge Isotope Laboratories, Inc.), *N,*

N-dimethylformamide (anhydrous, 99.8%, Aldrich), acetone (HPLC grade, Caledon), tetrahydrofuran (THF, ≥ 99.0%, Aldrich), thionyl chloride (≥ 99.0%, Aldrich), and methanol (HPLC, ≥ 99%, Caledon) were used as received. Poly(ethylene glycol) methyl ether (Me-PEG-OH, MW 2000 g/mol), sodium azide (NaN_3, ≥ 99.9% trace metals basis), pyridine (≥ 99.8%), *N,N'*-diisopropylcarbodiimide (DIC) (≥ 98.0%), hydroxybenzotriazole (HOBt), phthalimide, triphenylphosphine (Ph_3P, ≥ 98.5% GC), diisopropylazodicarboxylate (DIAD, ≥ 98%), hydrazine monohydrate (N_2H_4, 98%) were purchased from Aldrich and used as received.

3.2.2 Instrumentation

3.2.2.1 Nuclear Magnetic Resonance Spectroscopy

^1H NMR (Bruker 300 MHz high resolution NMR spectrometer) was used to characterize the products and reaction intermediates. Samples were prepared in either deuterated d_6-DMSO or $CDCl_3$. The terminal hydroxyl group of Me-PEG-OH appeared as a triplet around 4.5 ppm in the ^1H NMR spectrum acquired in d_6-DMSO[24,25] and its disappearance from the spectrum was used to determine the efficiency of the reaction between the terminal hydroxyl group and a given reagent. The disappearance of this signal was taken as strong evidence that Me-PEG-OH had been efficiently substituted at its terminal position.

3.2.2.2 Fourier Transform Infrared Spectroscopy

An FTIR spectrometer (Bruker Vector 22) was used to confirm the presence of an azide or amine group at one end of the PEG sample. Samples of the modified Me-PEG-OH were first dissolved

in DCM before being carefully deposited on a NaCl salt plate. The solvent was evaporated, leaving a homogeneous polymer film on the surface of the plate, which was used to acquire an FTIR spectrum.

3.2.2.3 Time-Resolved Fluorescence Measurements

The fluorescence decays for the quenching study were acquired with 20000 counts at the maximum of the instrument response function (IRF) and the fluorescence decay on an IBH time-resolved fluorometer equipped with a nanoLED light source. The IRF was convoluted with a sum of exponentials shown in Equation 3.1 and the result of the convolution was compared to the experimental decay.

$$[D^*]_{(t)} = [D^*]_{(t=0)} \times \sum_{i=1}^{n} a_i \times \exp(-t/\tau_i) \qquad 3.1$$

In Equation 3.1, a_i and τ_t represent the pre-exponential factors and the decay times, respectively. The quality of the fits was estimated from the χ^2 value (<1.13) and the random distribution of the residuals and the autocorrelation of the residuals.

3.3 Synthesis of Polymeric Quenchers

In order to conduct fluorescence quenching experiments on the Py-SNPs, a suitable quencher needed to be selected. In this study, a pyridinium cation and a nitro substituent which are known quenchers of the excited pyrene[16] were selected to prepare the Poly-Q samples. The synthesis protocols used to prepare the Poly-Qs are described hereafter.

3.3.1 Synthesis of Polymeric Quenchers

The first attempt at preparing a Poly-Q was carried out by attaching a pyridinium moiety to the end of Me-PEG-OH. To this end, Me-PEG-OH (1.56 g, 0.312 mmol) was dissolved in freshly distilled chloroform (20 mL) and the solution was placed in a three-neck round bottom flask that had been dried beforehand by flaming it under vacuum followed by purging it with N_2. Thionyl chloride (3 mL, 41.1 mmol) was then added into the solution under N_2. The reaction was left to react overnight with continuous stirring. After completion of the reaction, the solvent was evaporated under N_2 flow, yielding the green Me-PEG-Cl product. Me-PEG bearing a pyridinium chloride moiety (Me-PEG-PyrHCl) was obtained by reacting pyridine (40 µL, 5 mmol) and Me-PEG-Cl (1 g, 0.5 mmol) in 20 mL of acetonitrile for 6 hours at room temperature (r.t.). The final product was purified by dialysis against water, followed by three precipitations in cold ether in an ice bath, filtration, and drying under vacuum. The synthetic route is shown in Scheme 3.1. All reactions were conducted under a positive nitrogen pressure to prevent the introduction of moisture from the air.[26]

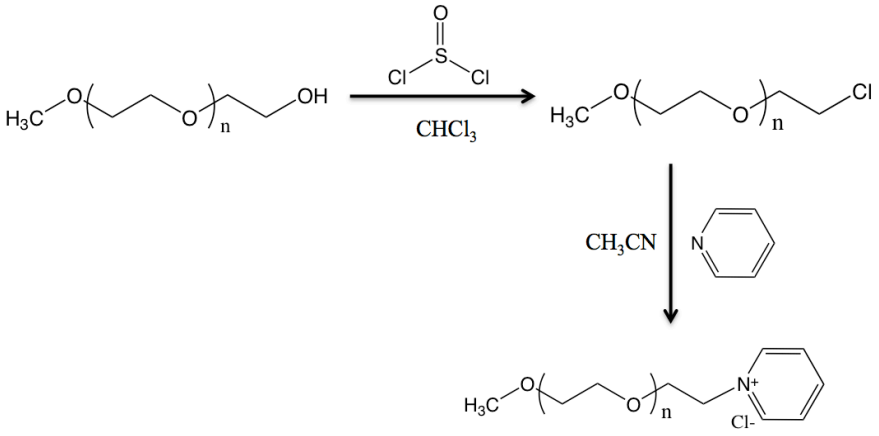

Scheme 3.1. Synthesis of PEG-PyrHCl.[26]

Beside the pyridinium moiety, the nitro group is also a suitable quencher for pyrene. Furthermore, being a neutral molecule, the nitro group possesses the additional advantage of not being subjected to unwanted electrostatic interactions with the charged SNPs that will be prepared at a later stage of the project. It is also less toxic to handle compared to pyridine. The target poly-Q was a PEG chain terminated at one end with a methyl group via an ether linkage and a nitropropane group at the other end via an amide bond to yield Me-PEG-C_3NO_2. The first step in the preparation of Me-PEG-C_3NO_2 shown in Scheme 3.2 consisted in replacing the hydroxyl group of Me-PEG-OH with a primary amine. Two synthetic routes were proposed to modify the end group of Me-PEG-OH. In the first method shown in Scheme 3.2, Me-PEG-OH (5 g, 2.5 mmol) was dissolved in freshly distilled toluene (50 mL), followed by the addition of thionyl chloride (4.3 mL, 59 mmol). The reaction was stirred overnight under N_2. The solvent was partially removed with a rotary evaporator before being precipitated in cold ether. The precipitation was repeated 3 times to remove any unreacted reagents, and the product was dried in a vacuum oven. Me-PEG-Cl (4 g, 0.88 mmol) was dissolved in freshly distilled DMF (40 mL), and sodium azide (NaN_3, 0.6 g, 9.2 mmol) was added to the solution. The temperature was increased to 80 ^oC and the solution was kept to react for 24 hours. All the processes were conducted under a positive nitrogen pressure. The reaction mixture was brought down to r.t. and the excess NaN_3 was filtered. The solution was precipitated into cold ether and dried in a vacuum oven. The azide group was then reduced to a primary amine by the Staudinger reduction[27] which is shown in Scheme 3.2.

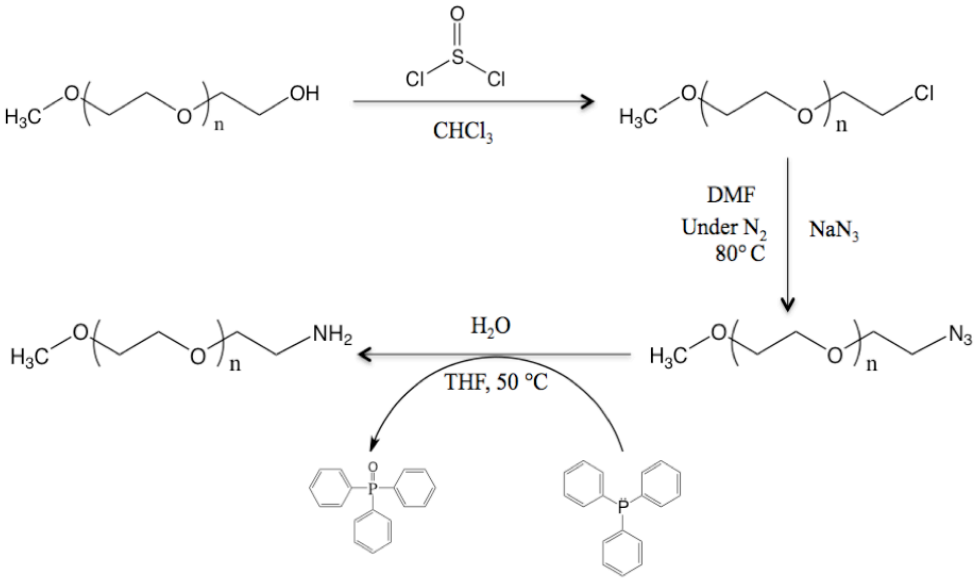

Scheme 3.2. Synthesis of PEG-NH_2 through the Staudinger reaction.[27]

However, sodium azide is sufficiently reactive that it could also react with the PEG backbone which would result in shorter chains. Since the molecular weight of Poly-Q is a key parameter to determine the mesh size of the crosslinked interior of the SNPs, it became important that the procedure used to prepare Me-PEG-C_3NO_2 should not affect the PEG backbone. Hence, a second method based on the Mitsunobu reaction was introduced in order to achieve this goal.[27] The Mitsunobu reaction is shown in Scheme 3.3. Me-PEG-OH (5 g, 2.5 mmol), triphenylphosphine (0.62 g, 10 mmol), and phthalimide (1.47 g, 10 mmol) were mixed at 0 ^oC in freshly distilled THF (50 mL) in a three-neck round bottom flask equipped with a magnetic stirrer. The mixture was stirred for 1 hour and diisopropyl azodicarboxylate (DIAD, 1.9 mL, 10 mmol) was added dropwise. The ice bath was removed after the addition of DIAD, and the reaction was allowed to stir for 24 hours. This process was conducted under N_2. The solvent was

partially removed and the solution was precipitated in cold ether. After conducting two additional precipitations, the product was dried under vacuum. The product Me-PEG-phthalimid (4 g, 2 mmol) and hydrazine monohydrate (5 mL, 65 mmol) were mixed in ethanol (40 mL) in a round bottom flask equipped with a magnetic stirrer. The solution was refluxed for 24 hours and the solvent was partially removed via rotary evaporation. The concentrated solution was precipitated into cold ether three times to yield a yellowish powder (3.5 g) of Me-PEG-NH_2 in 70% yield.[28]

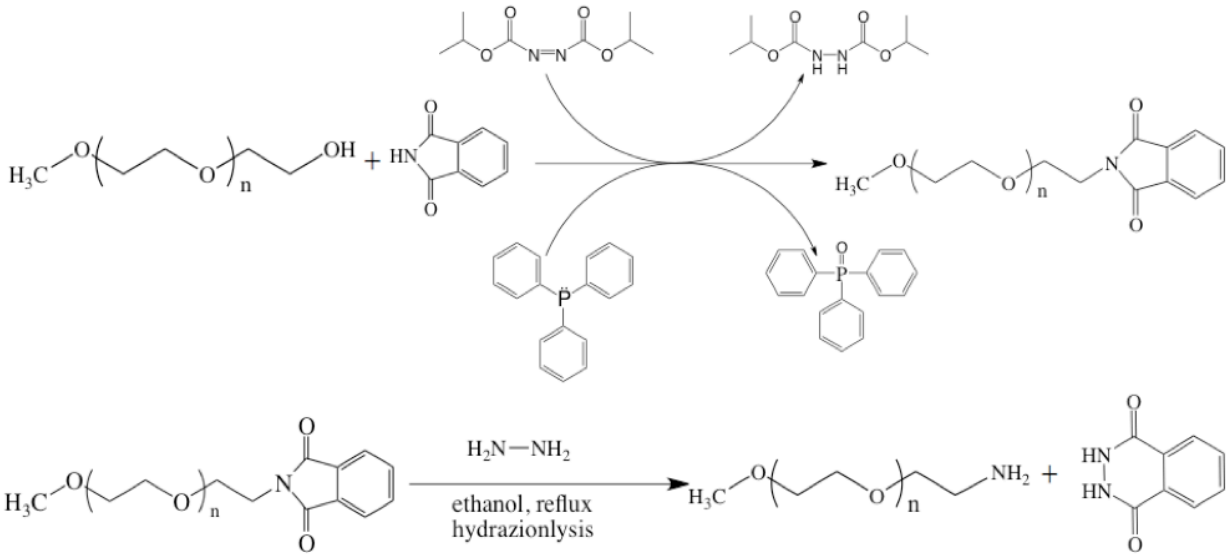

Scheme 3.3. Synthesis of Me-PEG-NH_2 based on the Mitsunobu reaction.[28]

The carboxylic acid of nitropropionic acid was reacted with the primary amine of Me-PEG-NH_2. Diisopropylcarbodiimide (DIC, 0.62 g, 3 mmol) was used as a coupling agent to react hydroxybenzotriazole (HOBt, 0.346 g, 3 mmol) with nitropropionic acid (0.36 g, 3 mmol) in DMF (10 mL) to form the activated intermediate for the final reaction. The synthesis procedure

is shown in Scheme 3.4. The reaction was stirred for 5 hours under N_2. The product was kept in solution without further purification to be used rapidly in the next reaction.

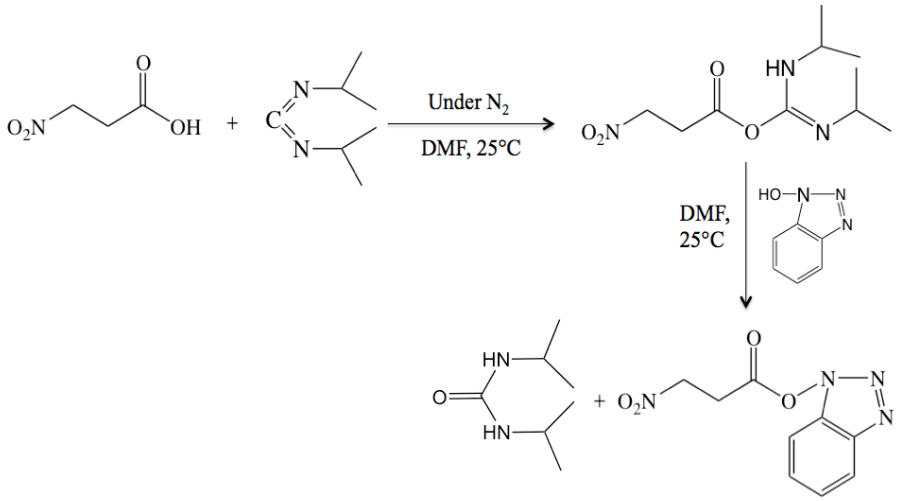

Scheme 3.4. Activation of nitropropionic acid with HOBt.[28]

The last step in the synthesis of Me-PEG-C_3NO_2 was to create the amide bond between PEO-NH_2 and the activated nitropropionic acid. The synthetic route is shown in Scheme 3.5.[29,30] Me-Me-PEG-NH_2 (1 g, 0.5 mmol) was dissolved into freshly distilled DCM (30 mL). The activated nitropropionic acid solution was added into the solution with an air tight syringe dropwise. The reaction mixture was stirred overnight. After completion of the reaction under N_2, the solvent was partially removed via rotary evaporation, followed by 3 precipitations of the final product into cold ether. The product was filtered and dried under vacuum yielding a yellowish colored powder (0.8 g) in 80% yield.

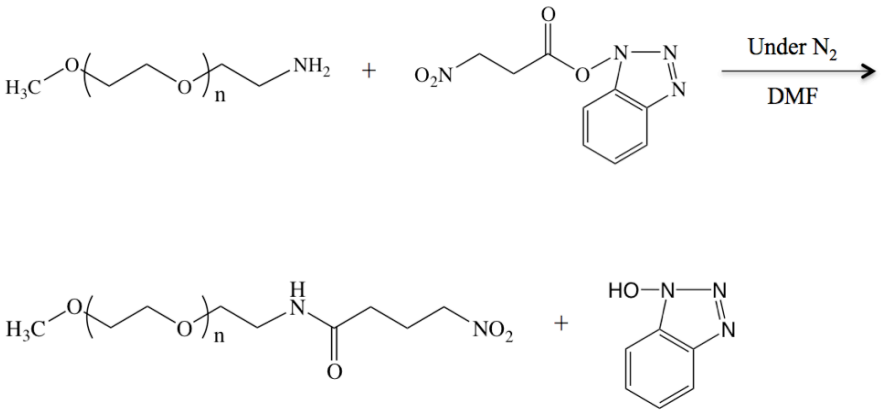

Scheme 3.5. Synthesis of Me-PEG-C_3NO_2.[26]

3.3.2 Characterization of Me-PEG-Pyridinium Chloride (PEG-PyrCl)

The ^{1}H NMR spectrum of Me-PEG-OH in DMSO is given in Figure 3.1 with the corresponding peak assignments. The triplet at 4.5 ppm belongs to the terminal hydroxyl group, and it was used to characterize the efficiency of the end group modification of Me-PEG-OH.[24]

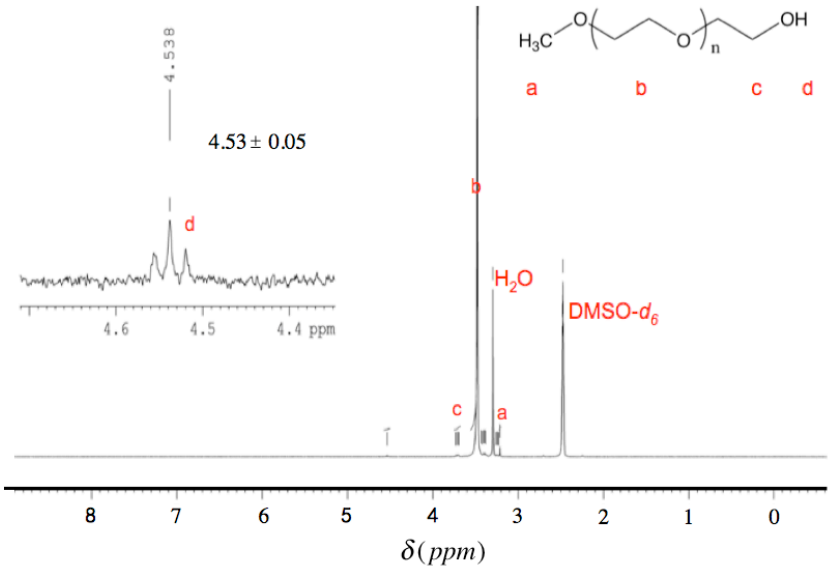

Figure 3.1. ^{1}H NMR spectrum of Me-PEG-OH in DMSO.

Me-PEG-OH was first chlorinated with thionyl chloride. The hydroxyl peak at 4.5 ppm disappeared after chlorination as shown in Figure 3.2.

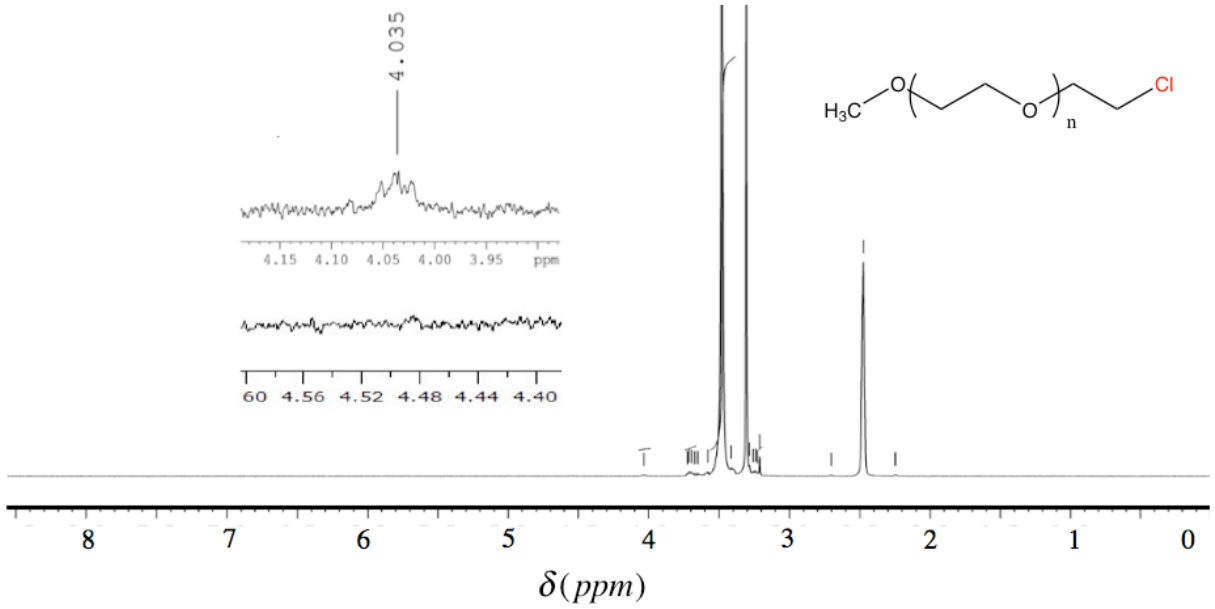

Figure 3.2. ^{1}H NMR spectrum of Me-PEG-Cl.

The ^{1}H NMR spectrum of PEO-PyrHCl is presented in Figure 3.3. Three new peaks appeared at 7.8, 8.3, and 8.8 ppm that belong to the *d*, *e*, and *f* protons of the aromatic ring of the pyridinium moiety.

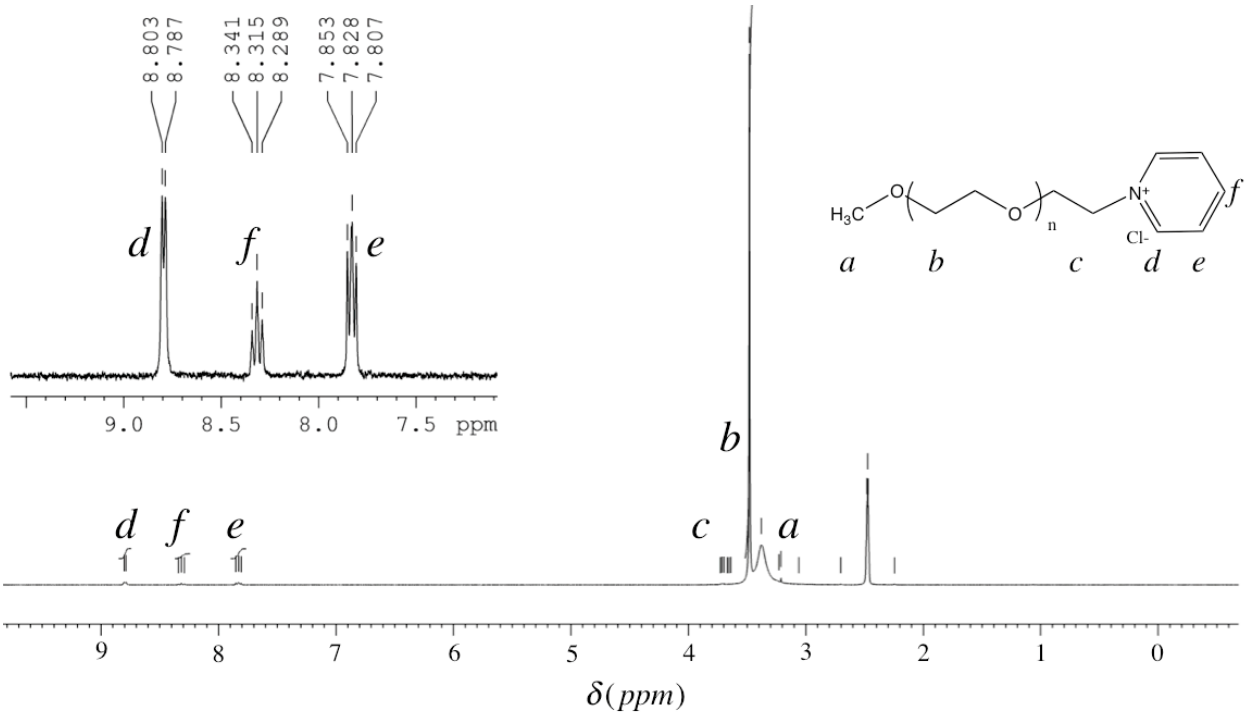

Figure 3.3. ^{1}H NMR spectrum of Me-PEG-PyrHCl.

In order to confirm the successful attachment of pyridine, the ^{1}H NMR spectrum of Me-PEG-PyrHCl was compared to that of pure pyridine and pyridine protonated with HCl in Figure 3.4. The position of the signal from the protons of pyridine and protonated pyridine was different from that of Me-PEG-PyrHCl. The comparison conducted in Figure 3.4 demonstrates that pyridine was successfully attached to the PEG chain. In order to quantify the fraction of PEG ends that had been labeled with pyridine, the product was freeze-dried to determine the pyridinium content of PEG-PyrHCl by UV-Vis absorption. However the sample was found to have decomposed after freeze-drying. The possible reason for the decomposition of Me-PEG-PyrHCl is that the C-N bond is not stable in aqueous solution. Since water will be used as a

solvent in the study of the SNPs, PEG-PyrHCl might not be the best candidate for the fluorescence quenching experiments. Hence another polymeric quencher was prepared with a more stable amide bond.

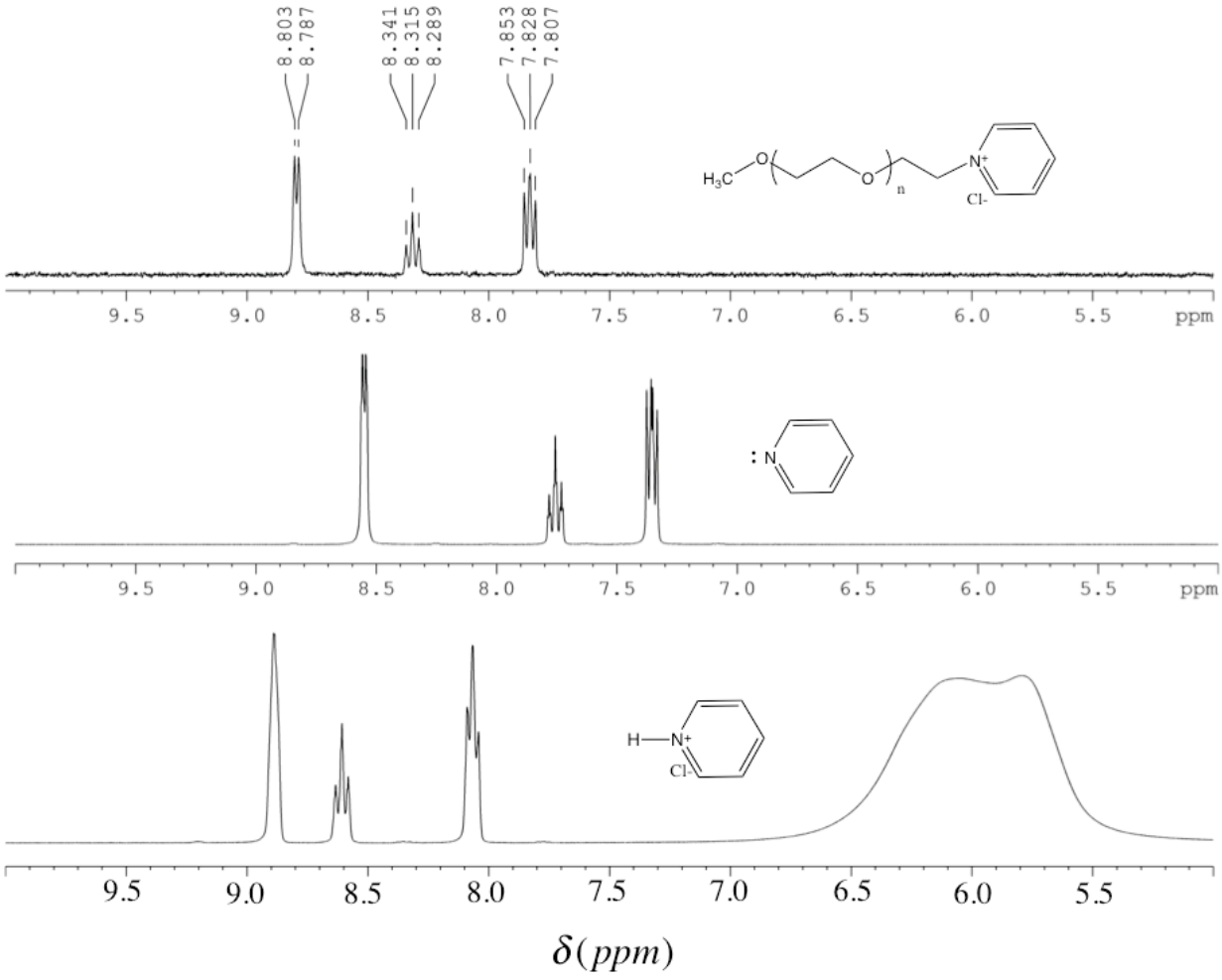

Figure 3.4. Comparison of the ^{1}H NMR spectra of Me-PEG-PyrHCl, pyridine, and protonated pyridine in d_6-DMSO.

3.3.3 Characterization of Me-PEG-C_3NO_2

Both FTIR and ^{1}H NMR spectroscopy were used to characterize the product of each reaction leading to the synthesis of Me-PEG-C_3NO_2. The FTIR spectra for PEG, Me-PEG-NH_2 and Me-PEG-C_3NO_2 are shown in Figure 3.5. The characteristic peaks of the key functional groups obtained for the different reaction intermediates have been assigned in the spectrum.

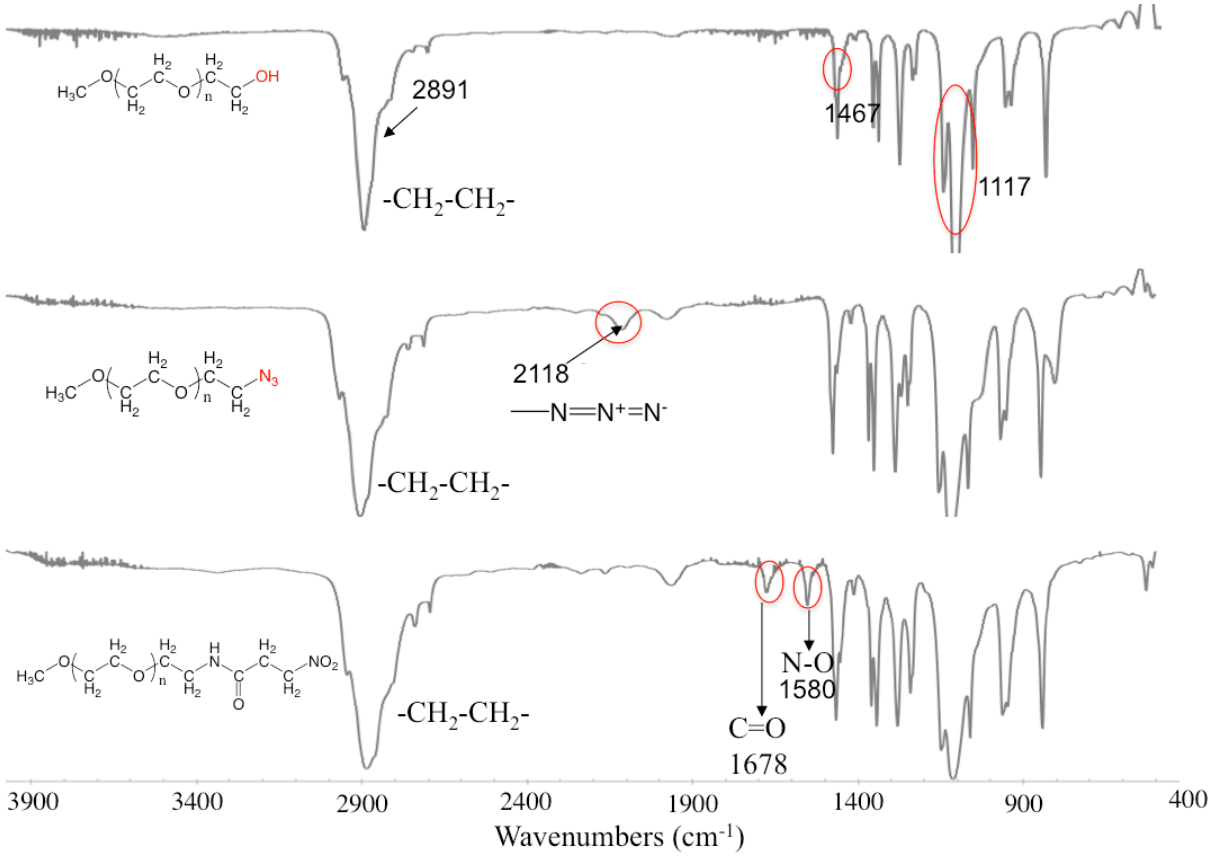

Figure 3.5. FTIR spectra of (top) Me-PEG-OH, (middle) Me-PEG-NH_2, and (bottom) Me-PEG-C_3NO_2.[28-30]

The large absorbance at 2891 cm^{-1} is from the -CH_2- stretch of the PEG backbone. The peak at 1467 cm^{-1} represents the C-H bond of the terminal methyl group of Me-PEG. The large

peak at 1117 cm^{-1} represents the C-O-C ether stretch from the PEG backbone.[27] These bands which pertain to the Me-PEG block are observed in the three FTIR spectra. The second FTIR spectrum was acquired with Me-PEO-N_3 for which the peak at 2118 cm^{-1} is characteristic of the azide group.[28] The bottom FTIR spectrum is that of Me-PEG-C_3NO_2. The peak at 1678 cm^{-1} shows the C=O stretch of the amide bond and the neighboring peak at 1580 cm^{-1} is from the N-O stretch of the nitropropionic acid.[29] The corresponding ^1H NMR spectrum of Me-PEG-C_3NO_2 with the corresponding peak assignment is given in Figure 3.6. The amide proton (d) appears at 8.09 ppm. The peaks at 2.7 and 4.7 ppm belong to the ethylene protons (e) and (f) of nitropropionic acid, respectively. The peak at 3.71 ppm represents the ethylene proton that is adjacent to the peptide bond. The large peak at 3.46 ppm represents the methylene protons (b) of the PEG backbone. The terminal methyl proton (a) of Me-PEG appears at 3.19 ppm, close to the water peak at 3.30 ppm.[24]

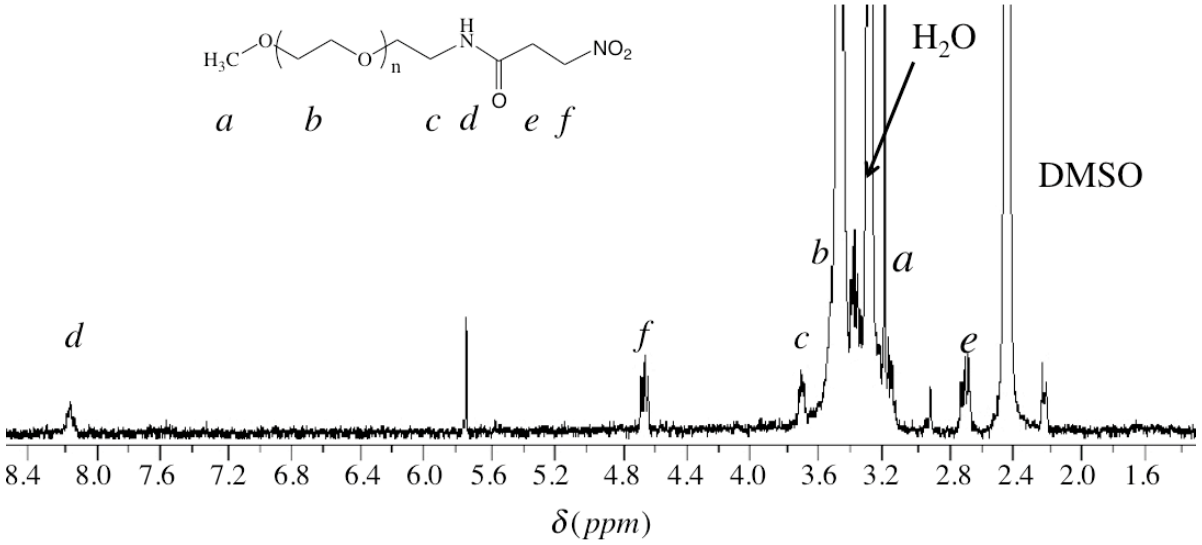

Figure 3.6. ^1H NMR spectrum of Me-PEG-C_3NO_2.

The Mitsunobu reaction was found to be more efficient in the synthesis of the amine terminated PEG. The successful conversion of Me-PEG-OH into Me-PEG-Phthalimide is proven by the complete disappearance of the terminal hydroxyl group at 4.5 ppm from the ^{1}H NMR spectrum shown in Figure 3.7 and the appearance of a new peak from the benzylic protons of Me-PEG-Phthalimide at 7.8 ppm. The yield of this reaction was 90%. After the hydrazinolysis, the signal at 7.8 ppm disappeared. Instead, the $-NH_2$ signal of Me-PEG-NH_2 appeared at 2.8 ppm, and the yield for that step was 82%. The coupling reaction with nitropropionic acid had a yield of 64%. The ^{1}H NMR spectra was shown in Figure 3.7 with the assignments of each functional group.[28]

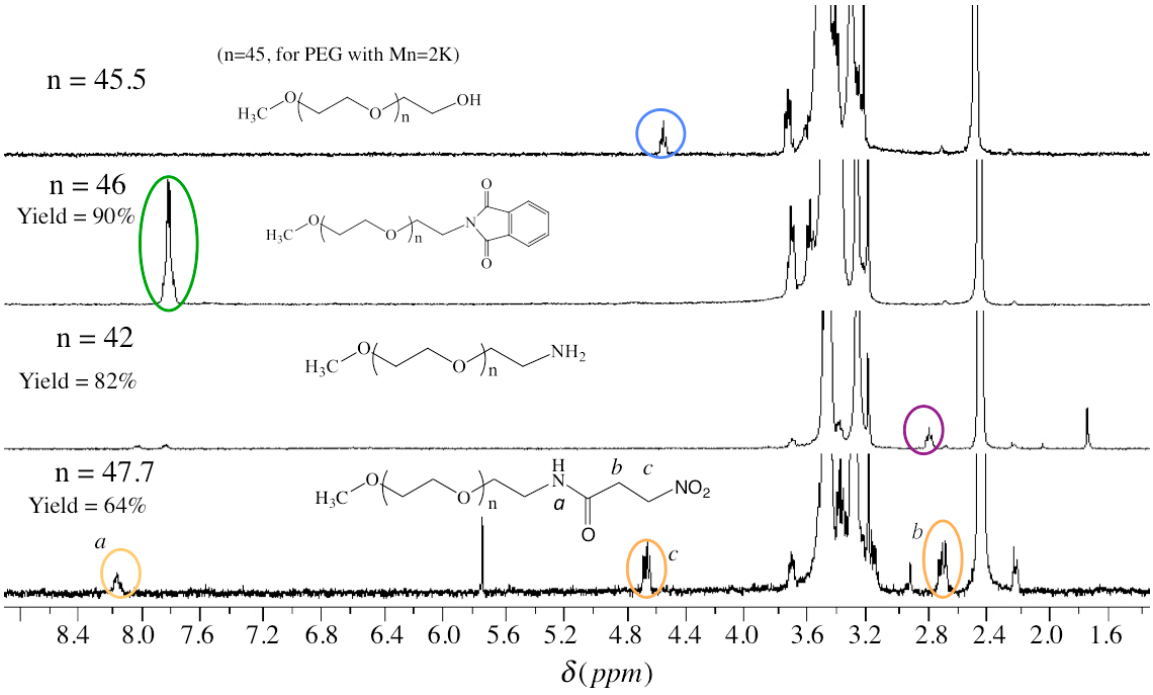

Figure 3.7. ^{1}H NMR spectra of (top) Me-PEG-OH (M_n = 2K, DP = 45) as received from Aldrich, (second from top) Me-PEG-Phthalimide after the Mitsunobu reaction, (second from

bottom) Me-PEG-NH_2 after hydrazinolysis of the PEG-Phthalimide, and (bottom) Me-PEG-C_3NO_2 after the coupling reaction with 3-nitropropionic acid.[27]

3.4 Fluorescence Quenching Experiments

The successful synthesis of Me-PEG-C_3NO_2 opened the way to conduct fluorescence quenching experiments on the pyrene-labeled SNPs. These experiments are described hereafter.

3.4.1 Quenching with Nitromethane

The quenching efficiency of the nitro group in DMSO was estimated by conducting fluorescence quenching experiments with PMe(0.05)-SNP0 (SNP0 labeled with 0.05 mol% of 1-pyrenemethanol) and 1-pyrene-methyl ether ($PyCH_2OCH_3$) with nitromethane. The fluorescence spectra and decays of PMe(0.05)-SNP0 and $PyCH_2OCH_3$ with a 2.5 μM pyrene concentration in DMSO were acquired at different nitromethane concentrations. As shown in Figure 3.8, the fluorescence intensity decreased continuously with increasing concentrations of nitromethane for both solutions of PMe(0.05)-SNP0 and $PyCH_2OCH_3$ in DMSO.

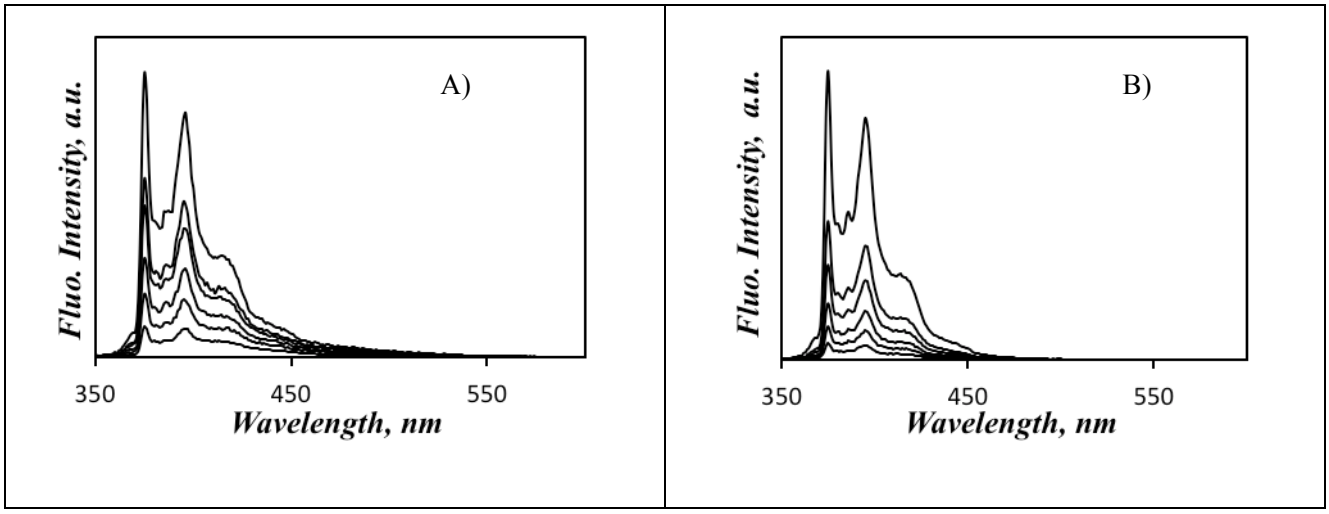

Figure 3.8. Fluorescence spectra of A) PMe(0.05)-SNP0 and B) $PyCH_2OCH_3$ in DMSO quenched by nitromethane. [Py] = 2.5 μM, λ_{ex} =346 nm.

The ratio I_0/I of the fluorescence intensity of pyrene without nitromethane (I_0) over that with nitromethane (I) was plotted as a function of nitromethane concentration in Figure 3.9. This plots, also referred to as Stern-Volmer plots, were linear. In the absence of static quenching, the slope of these plots equals the product $k_Q \times \tau_M$ where k_Q is the bimolecular rate constant for pyrene quenching by nitromethane and τ_M is the natural lifetime of the PyMe-O labels in aerated solutions of DMSO. Since τ_M was estimated to equal 97 ns, k_Q was found to equal 3.4×10^9 and 1.6×10^9 $M^{-1}s^{-1}$ for $PyCH_2$-O-CH_3 and PMe(0.05)-SNP0, respectively. The smaller k_Q value obtained for the Py-SNPs reflects the lower mobility of pyrene after being covalently attached onto a much larger SNP.

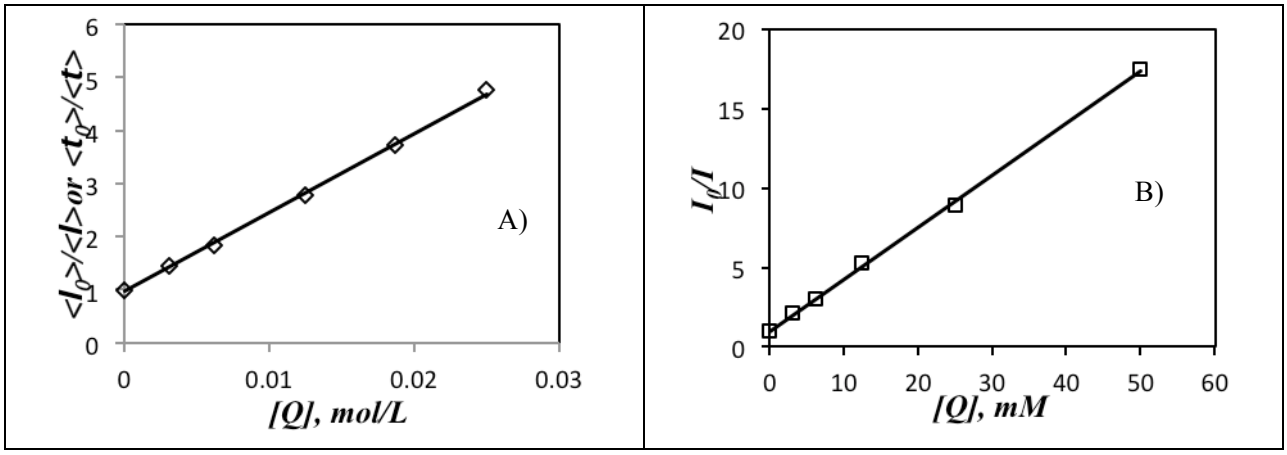

Figure 3.9. Plot of the I_0/I ratio as a function of quencher concentration. A) PMe(0.05)-SNP0 and B) $PyCH_2$-O-CH_3.

The fluorescence decays of the PMe(0.05)-SNP0 solutions used to acquire the fluorescence spectra in Figure 3.8 were obtained. They were fitted with a sum of two exponentials according to Equation 3.1 to obtain the number-average decay time $<\tau>$. The decay times and pre-exponential factors retrieved from this analysis are listed in Table 3.1.

Table 3.1. Pre-exponential factors and decay times obtained from the biexponential analysis of the fluorescence decays of PMe(0.05%)-SNP0 in aerated DMSO solutions.

[Q] mmol/L	a_1	τ_1	a_2	τ_2	$<\tau>$	χ^2	$<\tau_0>/<\tau>$
0	0.09	33.9	0.91	96.1	90.5	0.95	1
3.2	0.13	29.1	0.87	70.3	64.8	1.05	1.4
6.4	0.18	25.1	0.82	56.1	50.2	1.15	1.8
12.6	0.29	21.6	0.72	40.9	35.4	1.23	2.6
18.7	0.46	19.4	0.54	34.0	27.3	1.05	3.3
24.8	0.50	15.8	0.50	28.6	22.2	1.07	4.1

The ratio $<\tau_0>/<\tau>$ was plotted as a function of quencher concentration. The $<\tau_0>/<\tau>$ plot in Figure 3.10 was compared to the I_0/I plot obtained from steady-state fluorescence. The slope of the I_0/I ratio is 20% larger than that of $<\tau_0>/<\tau>$, thus indicating residual static quenching.

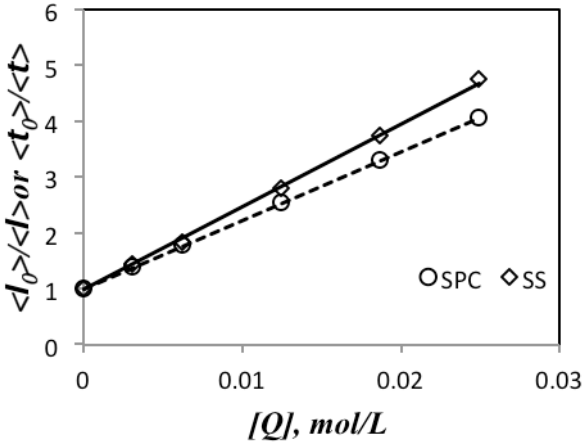

Figure 3.10. Stern-Volmer plots of the I_0/I (◊) and $<\tau_0>/<\tau>$ (O) ratios as a function of nitromethane concentration for PMe(0.05)-SNP0.

3.4.2 Fluorescence Quenching with Me-PEG-C_3NO_2

The fluorescence spectra and decays of a 1.7 g/L solution of PMe(0.05)-SNP0 in aerated DMSO were acquired as a function of Me-PEG-C_3NO_2 concentration. The fluorescence quenching experiments were conducted at room temperature. A concentrated solution of Me-PEG-C_3NO_2 (9.74 mmol/L) was added to the PyMe(0.05)-SNP0 solution via a 100 μL syringe to obtain various quencher concentrations in DMSO. After each quencher injection, the solution was allowed to equilibrate for 5 min before acquiring a fluorescence spectrum and decay. The

fluorescence spectra are shown in Figure 3.11. The fluorescence intensity decreases with increasing concentration of polymeric quencher, as expected.

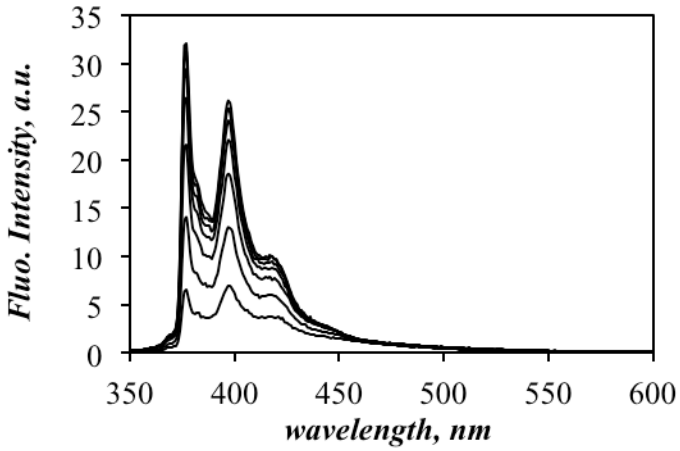

Figure 3.11. Fluorescence spectra at room temperature with increasing concentration of polymeric quencher.

The fluorescence spectra shown in Figure 3.11 were analyzed to generate the Stern-Volmer plot shown in Figure 3.12.

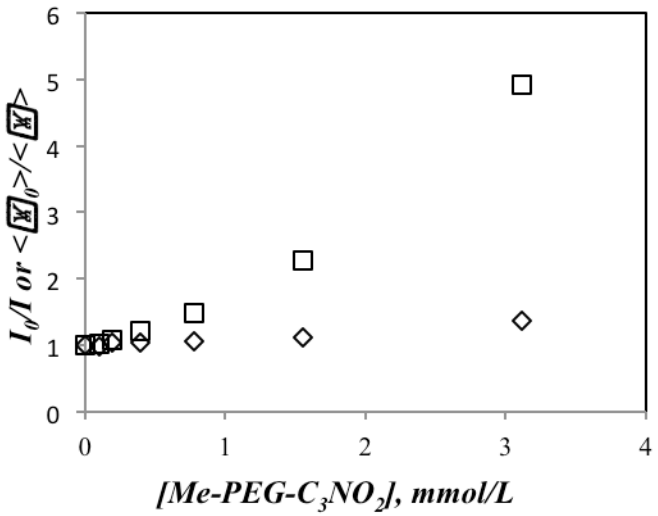

Figure 3.12. Stern-Volmer plot of the I_0/I (□) and $\langle\tau_0\rangle/\langle\tau\rangle$ (◊) ratio as a function of quencher concentration.

The I_0/I plot showed an upward curvature, suggesting that the fluorophore was subject to both collisional and static quenching. The fluorescence decays acquired with the solution used to obtain the fluorescence spectra in Figure 3.11 were fitted with a sum of two exponentials. The number average decay time $\langle\tau\rangle$ of the fluorescence decays was calculated and the ratio $\langle\tau_0\rangle/\langle\tau\rangle$ was plotted as a function of quencher concentration in Figure 3.12. By increasing the Me-PEG-C_3NO_2 concentration up to 3.1 μM, the $\langle\tau_0\rangle/\langle\tau\rangle$ ratio increased by less than 40 % whereas the I_0/I ratio increased 5-fold. This result was a bit surprising as the I_0/I and $\langle\tau_0\rangle/\langle\tau\rangle$ yielded similar trends for the quenching of PMe(0.05)-SNP0 by nitromethane in Figure 3.10. The reason for this different behavior observed with Me-PEG-C_3NO_2 is that it absorbs strongly at 346 nm where the pyrene label absorbs, as observed in Figure 3.13.

In fact, the molar absorbance coefficient at 346 nm of Me-PEG-C_3NO_2 is comparable to that of nitromethane. But since Me-PEG-C_3NO_2 diffuses much more slowly than nitromethane, larger amounts of Me-PEG-C_3NO_2 are required to achieve an appropriate quenching. Unfortunately, these large concentrations of polymeric quencher result in a large absorption, which leads to a decrease in fluorescence intensity that is not due to quenching. This effect represents an artifact that prevents the completion of the fluorescence quenching experiments. Consequently, this project was abandoned.

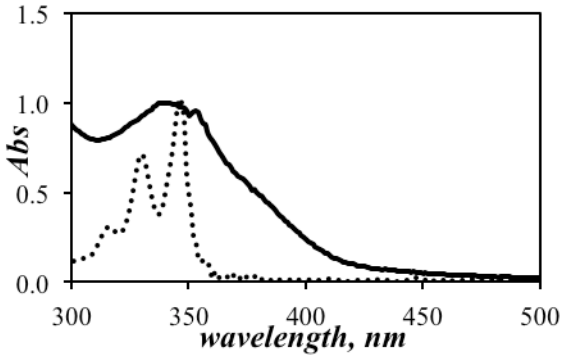

Figure 3.13. UV-Vis absorption spectra of a 0.85 g/L PMe(0.05)-SNP0 solution in DMSO (···) and a 6 g/L PEG-C_3NO_2 solution in DMSO (—).

Table 3.2 Pre-exponential factors and decay times obtained from fitting the fluorescence decay of PMe(0.05)-SNP0.

sample	[py], μmol/L	[PEG-Q], mmol/L	$<\tau_0>/<\tau>$	I_0/I
0	2.5	0	1	1
1	2.5	0.097	1	1.03
2	2.5	0.195	1.04	1.09
3	2.5	0.39	1.05	1.22
4	2.5	0.78	1.07	1.49
5	2.5	1.56	1.13	2.28
6	2.5	3.12	1.38	4.92

3.5 Conclusions

Two types of PEG-based polymeric quenchers (Me-PEG-PyrHCl and Me-PEG-C_3NO_2) were successfully synthesized. Me-PEG-PyrHCl was found to degrade over time in water and was thus quickly discarded. The synthesis of Me-PEG-C_3NO_2 proceeded by preparing an amine-terminated PEG (Me-PEG-NH_2) which was reacted with nitropropionic acid to covalently link the nitropropane group with an amide bond. Me-PEG-NH_2 was synthesized by either replacing the terminal hydroxyl of Me-PEG-OH by an azide group that was later reduced to the amine, or by applying the Mitsunobu reaction. Having established a robust procedure to prepare Me-PEG-C_3NO_2, fluorescence quenching experiments were conducted whereby the pyrene labels of Py-SNPs were quenched by the nitro group of Me-PEG-C_3NO_2. Unfortunately the decrease in mobility experienced by the pyrene labels and the nitro groups following their attachment to large macromolecules led to a massive reduction in the quenching of the pyrene labels by Me-PEG-C_3NO_2. To achieve a detectable quenching, large concentrations of Me-PEG-C_3NO_2

needed to be used. Unfortunately, the weak absorbance of Me-PEG-C_3NO_2 became a problem at the large concentrations of polymeric quencher that needed to be used. As a result, no further quenching experiments were conducted.

Chapter 4

Probing the Deformability of SNPs by Pyrene Fluorescence and Transmission Electron Microscopy

4.1 Introduction

The main current commercial application of SNPs is for paper coating whereby a concentrated SNP suspension is applied to the surface of paper. As water evaporates, the SNPs aggregate to form a continuous and smooth film on top of the rough paper surface generated by the cellulose fibers. During film formation, two phenomena are most likely to happen. In the first case, the SNPs constituted of branched amylopectin could be viewed as structurally opened particles, which would enable them to interpenetrate effectively and create a homogenous film. In the second case, the branched and rigid amylopectin chains would create a particle interior that is too sterically hindered to allow interparticle diffusion. Under such conditions, the SNPs would shrink continuously as the solvent evaporates and the film would be constituted of individually collapsed SNPs held together by peripheral van de Waals interactions.

The purpose of this chapter was to provide experimental evidence that SNPs can undergo substantial deformation under some specific conditions, particularly in the semi-dilute regime that corresponds to the range of SNP concentrations used in paper coating applications. A technique capable of achieving this goal should be able to probe changes in particle volume in the nanometer scale, since the SNPs have a diameter that ranges from 10 to 50 nm depending on the amount of crosslinking agent used during extrusion. Furthermore, this technique would possess the ability to isolate a single SNP from a sea of others and assess how its volume is affected by the presence of the other SNPs. In this context, the characterization of the process of pyrene excimer formation in Py-SNPs appears to be particularly well-suited to fulfill these experimental requirements. First, the fluorescence signal of the Py-SNPs is strong enough to

enable the study of isolated emitting Py-SNPs out of a background of non-fluorescent SNPs. Second, pyrene excimer formation depends strongly on the local pyrene concentration $[Py]_{loc}$ within a pyrene-labeled macromolecule. Thus, compression of a macromolecule results in an increase in $[Py]_{loc}$, and consequently, an increase in excimer formation.

The Py-SNPs were used in two different manners to demonstrate the plasticity of the SNPs. In the first experiment, excimer formation in Py-SNPs was monitored as a function of the concentration of unlabeled SNPs. The massive increase in overall solution viscosity as the SNP concentration was increased from 10 to 800 g/L should have led to a corresponding reduction in excimer formation via diffusive encounters. On the contrary, excimer formation increased close to two folds, thus demonstrating an increase in $[Py]_{loc}$ and thus an unexpected reduction in the macromolecular volume of the Py-SNPs with increasing SNP concentration. The plasticity of the SNPs was further confirmed by using fluorescence and transmission electron microscopy (TEM) to probe the hydrophobic collapse of the Py-SNPs induced by the intramolecular aggregation of the pyrene labels in aqueous solution. Together, the fluorescence and TEM measurements described in this chapter provide strong evidence that the SNPs are capable of undergoing substantial deformation under an external stress.

4.2 Experimental procedure

4.2.1 Instrumentation

4.2.1.1 Viscometry

Intrinsic viscosity measurements were performed using two Cannon D449 Dilution Ubbelohde viscometers of size 100 and 200 used with Mili-Q water (η = 0.89 mPa•s at 25 °C) and DMSO (η = 1.99 mPa•s at 25 °C), respectively. A circulating water bath was used to keep the temperature of the viscometer steady at 25 °C during the intrinsic viscosity measurements.

4.2.1.2 Steady-State Fluorescence

Steady-state fluorescence spectra of the PBA(2.5)-SNP0 sample where 2.5 mol% of the glucose units of SNP0 were labeled with 1-pyrenebutyric acid (PBA) were obtained with a PTI LS-100 steady-state fluorometer which was equipped with an Ushio UXL-75Xe Xenon arc lamp and a PTI 814 photomultiplier detection system. All the fluorescence measurements were conducted with the front face geometry in a triangular quartz cell. The samples were excited at 346 nm. The monomer fluorescence intensity (I_M) was obtained by integrating the fluorescence spectrum from 372 to 378 nm, while the excimer fluorescence intensity (I_E) was determined by integrating the spectrum from 500 to 530 nm.

4.2.1.3 Time-Resolved Fluorescence Measurements

The fluorescence decays of the Py-SNPs were obtained with an IBH time-resolved fluorometer equipped with a nanoLED light source. The front face geometry was also adopted for the decay

acquisition. The solutions were excited at 346 nm and the decays were acquired at 375 nm and 510 nm for the monomer and excimer using a cut-off filter at 370 and 495 nm, respectively.

4.2.1.4 Transmission Electron Microscopy

The TEM images were acquired with a Philips CM10 transmission electron microscope equipped with an AMT digital camera. The high tension (HT) range was between 40 to 100 kV, and the resolution of the objective lens equaled 0.5 nm for a point and 0.34 nm for a line. This instrument allowed a magnification ranging from 20 to 450000X.

4.2.2 Sample preparation

4.2.2.1 Intrinsic Viscosity

For each sample, 5 solutions with different SNP concentrations ranging from 1 mg/L to 10 mg/L were prepared. The minimum volume required for the Ubbelohde viscometer was 8 mL. The set up consisted of the Ubbelohde viscometer immersed in a water bath where the temperature was set to equal 25 °C based on the reading of a thermometer situated in the water bath at a location close to the viscometer. After filling the viscometer with the SNP solution, the set up was allowed to equilibrate for about 10 mins before conducting a measurement.

4.2.2.2 Preparation of the SNP Solutions in the Semi-dilute Regime

Nine samples containing different amounts of unlabeled SNPs (from 0.17 g/L to 800 g/L) were prepared. For samples with concentration of naked SNPs of less than or equal to 200 g/L, the solutions were prepared by weighing the required amount of naked SNPs in a vial and adding to the vial a pre-determined mass of a solution of PBA(2.5)-SNP0 with an absorbance at 346 nm

equal to 1. This absorbance corresponded to a pyrene concentration of 25 μM and a massic concentration of PBA(2.5)-SNP0 of 0.17 g/L. This absorbance was selected to ensure that the pyrene labels would be dilute enough to prevent intermolecular excimer formation, but that the fluorescence signal would be strong enough to acquire a decent fluorescence spectrum. Solutions prepared in such manner were stirred for at least 24 hours until the polymer was homogeneously dispersed.

For SNP concentrations higher than 200 g/L, samples were prepared by weighing the required amount of naked SNP in a vial and adding to the vial a measured quantity of Py(2.5)-SNP0 solution in DMSO with a 0.5 OD at 346 nm. The solvent was partially removed by continuously blowing N_2 into the vial until half of the volume had evaporated. The volume of the SNP solution was measured as follows. DMSO was added to another empty vial until the meniscus of the DMSO matched that of the vial containing the SNP dispersion. Using the mass of the DMSO added to the second vial, the volume of DMSO added was determined from the density of the DMSO at 25 ^{o}C which equals 1.1 g/mL. The PBA(2.5)-SNP0 solutions were not degassed since pyrene has a relatively long lifetime (~100 ns) in DMSO. For SNP concentrations greater than 200 g/L, the solution was too viscous to be transfer into the cell. Hence an aliquot of the solution was simply pasted onto the inner surface of the cell.

4.2.2.3 PBA(5)-SNP0 DMSO Sample Preparation for TEM Measurements

Two types of TEM grids (Electron Microscopy Sciences) were employed depending on the solvent used to prepare the PBA(5)-SNP0 solution. For samples prepared in water, a 400 mesh copper grid coated with formvar film was employed to conduct the TEM experiments while a

200 mesh copper grid coated with carbon film was used for the samples prepared in DMSO. A 0.5 mg/L PBA(5)-SNP0 solution (10 μL) was cast onto the TEM grid. The solvent was evaporated under vacuum at 50 ^{o}C for 24 hours for DMSO and at room temperature for 12 hours for water.

After the solvent had evaporated, the sample was stained by exposing the grid to a 0.5 w/w% ruthenium tetroxide (RuO_4) solution in water (Electron Microscopy Sciences). RuO_4 is a commonly used staining agent for starch and aromatic compounds.[35] The copper grid was placed at the center of a 2 cm × 2 cm parafilm square. The film with the copper grid was placed in a petridish and 4 drops (50 μL) of RuO_4 solution were deposited in each corner of the film. The petridish was covered with a lid and the SNP sample was exposed to the RuO_4 fumes for 40 s, before being transferred to another clean petridish. For the best imaging results, the stained samples were characterized 2-12 hours after staining. Ruthenium tetroxide is a strong oxidizing agent that is volatile and quite toxic even at the low concentration of 0.5 w/w% used in these experiments. The vapors are irritating to the eyes and the respiratory tract. Hence the staining process was done in the fume hood and protective goggles and gloves were worn at all times. Since RuO_4 reacts violently with filter paper and alcohol, ruthenium tetroxide waste needed to isolated and processed separately.[35]

4.3 Results and Discussion

4.3.1 Intrinsic Viscosity

Although the SNPs are typically dispersed in water, the pyrene label, being highly hydrophobic, strongly reduces the solubility of the Py-SNPs in water and induces their aggregation. Consequently, the fluorescence experiments were carried out in DMSO where pyrene and the SNPs are soluble. The solution properties of the naked SNPs were compared in DMSO and water by conducting intrinsic viscosity experiments.

The flow time of each SNP solution was measured at least 4 times in order to generate one data point, and 5 data points were determined to calculate the intrinsic viscosity. One example is shown in Figure 4.1.

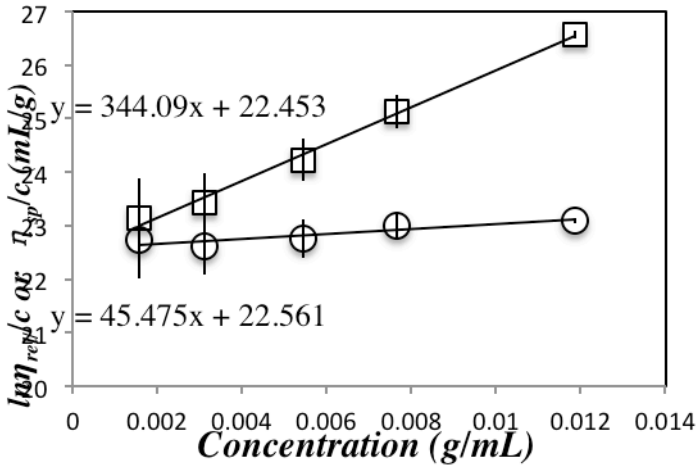

Figure 4.1. Plot of (□) $\ln(\eta/\eta_0)/[poly]$ and (O) $(1-\eta/\eta_0)/[poly]$ for SNP5 in DMSO at 25 °C.

The plots of $(1 - \eta/\eta_0)/[poly]$ and $\ln(\eta/\eta_0)/[poly]$ versus polymer concentration could be well approximated by two straight lines which, after extrapolation to zero polymer concentration,

intercepted the y-axis at the same value of 22.5 ± 0.1 mL/g, which was taken as the value of [η] for this sample. The intrinsic viscosity of all SNPs were measured in both DMSO and water. They were plotted in Figure 4.2A as a function of the weight fraction of crosslinker used in the extrusion process. [η] was found to decrease rapidly with increasing amount of crosslinker used during extrusion up to a crosslinker level of 2 w/w%. For particles with crosslinker levels greater than 2 w/w%, no change in [η] was observed and [η] took values of 20 ± 6 mL/g and 13 ± 4 mL/g in DMSO and water, respectively. By plotting the ratio of the intrinsic viscosities of the SNPs in DMSO and water as a function of crosslinker w/w% in Figure 4.2B, it was found that the SNPs had [η] values in DMSO that were about 1.7 ± 0.2 times larger than in water, suggesting that they were better solvated in DMSO. This enhancement in solubility will have to be accounted for when results obtained by fluorescence on the Py-SNPs in DMSO are used to predict how the SNPs behave in aqueous solution

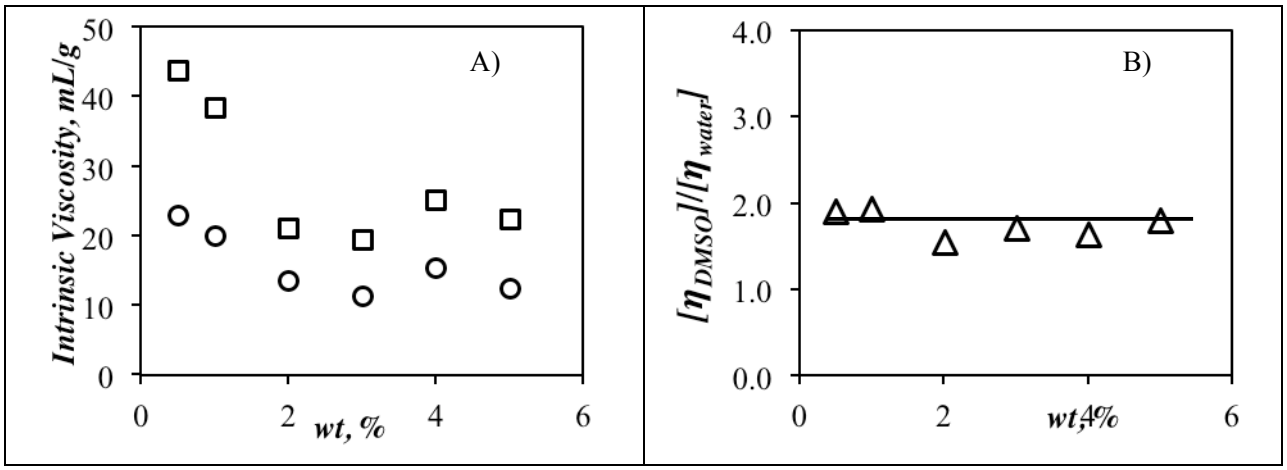

Figure 4.2. Plots of A) [η] in (□) DMSO and (○) water B) of the ratio $[\eta_{DMSO}]/[\eta_{H2O}]$ both as a function of the weight fraction (wt%) of crosslinker used in the extrusion.

4.3.2 Characterization of the Semidilute Solutions of PBA(2.5)-SNP0

The fluorescence spectra of all PBA(2.5)-SNP0 solutions were acquired as a function of the concentration of the non-fluorescent SNPs, as shown in Figure 4.3. The spectra were normalized at the 0-0 peak at 375 nm.

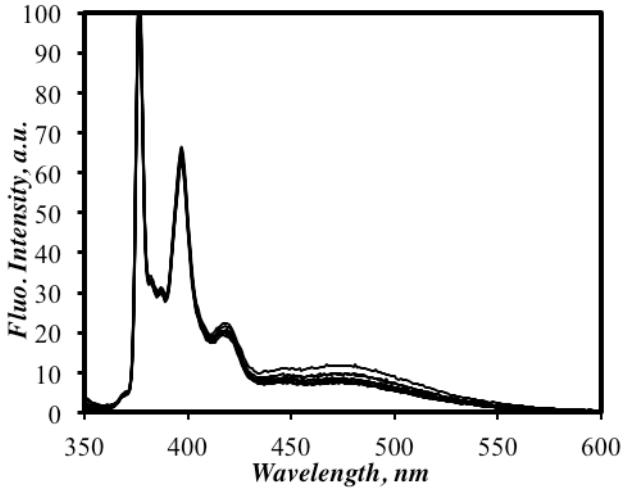

Figure 4.3. Fluorescence spectra of PBA(2.5)-SNP0 excited at 346 nm. The unlabeled SNP concentration is increased from 0 g/L (bottom trace) to 800 g/L (top trace).

With the increase of the concentration of the unlabeled SNP, the excimer fluorescence increased substantially. This phenomenon was described by the I_E/I_M ratio. As shown in Figure 4.4A, the I_E/I_M ratio remained constant when the SNP0 concentration was below 10 g/L, and then increased dramatically at concentration higher than 100 g/L. The increase of the I_E/I_M ratio indicates that more excimer was being formed at higher SNP0 concentration. This phenomenon was quite unexpected because, as the concentration of the polymer increased, the solution

became highly viscous, and chain motion should have been slowed down due to the high local viscosity. Hence, the I_E/I_M ratio should have decreased with increasing polymer concentration. The data in Figure 4.4A were used to generate a log-log plot of I_E/I_M versus SNP0 concentration in Figure 4.4B. Above a SNP0 concentration of 48 g/L, ln I_E/I_M increased linearly with increasing ln[SNP0] with a slope of 0.22. This result implies that I_E/I_M scales as $[SNP0]^{0.22}$. The increase in I_E/I_M occurs at an SNP0 concentration that is past the overlap concentration C* of SNP0 estimated to equal $C^* = [\eta]^{-1} = 16$ g/L. This concentration range belongs to the semi-dilute regime where polymer coils interpenetrate and chains form entanglements. In the case of linear polymers, an excess of unlabeled polymer added to a dilute solution of a pyrene-labeled polymer results in a decrease in I_E/I_M due to the formation of entanglements at concentration above C*.[36] That a decrease in I_E/I_M is not observed with the SNPs suggests that SNPs do not entangle but rather decrease in size above C* in a process that brings the pyrene labels closer from each other, enhances pyrene-pyrene encounter, and favors excimer formation.

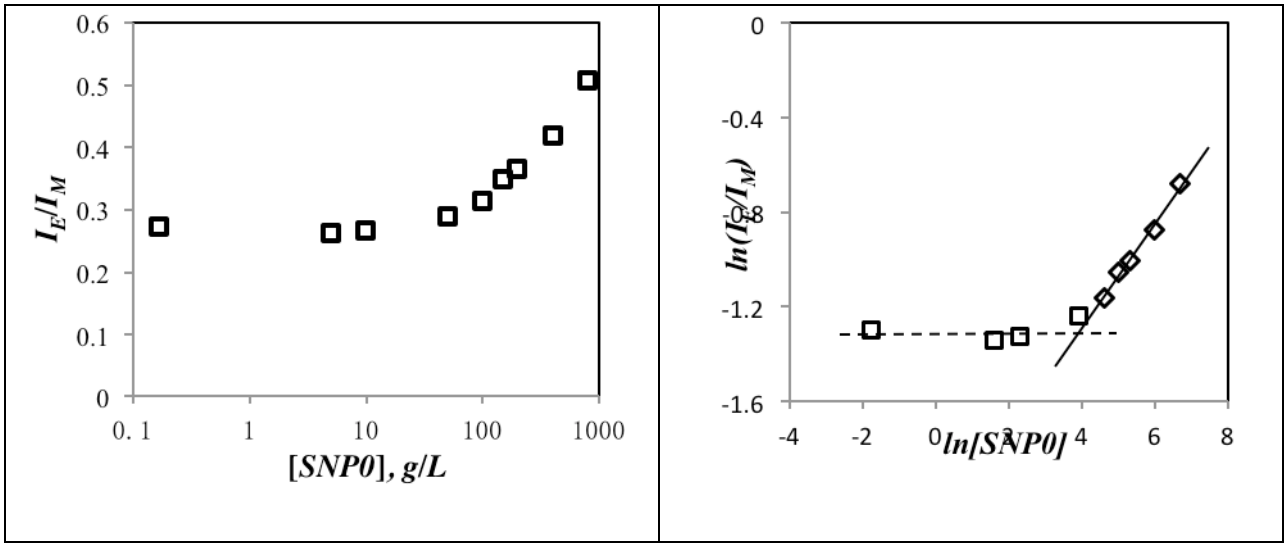

Figure 4.4. A) Plot of I_E/I_M ratio as a function of naked SNP concentration; B) Plot of ln(I_E/I_M) as a function of ln[SNP0].

The contraction of the SNPs above C* can be rationalized by considering the osmotic pressure generated by the solvent inside the SNPs. At C*, the surface of the SNPs is in contact with that of other SNPs. Soft and highly deformable polymer coils of linear chain would interpenetrate above C*, but the rigid and branched SNPs do not. This situation creates a dense starch-rich, and thus solvent-poor, region at the surface of the SNPs, thus creating a chemical potential gradient for the solvent molecules that decreases from the SNP center to their surface. To counteract this chemical potential gradient, the solvent molecules located inside the SNPs diffuse outwards to their surface resulting in a decrease of the SNP volume, and thus an increase in the I_E/I_M ratio.

4.3.3 Characterization of PBA(5)-SNP0 by Steady-State and Time-Resolved Fluorescence

The steady-state fluorescence spectra of dilute PBA(5)-SNP0 solutions were acquired in both DMSO ([Py] = 2.5×10^{-6} M) and water ([Py] = 2.5×10^{-7} M) as shown in Figure 4.5. The typical monomer emission peaks are observed in the 370-425 nm wavelength range, while the excimer fluorescence appeared as a broad structureless emission centered at around 470 nm. Analysis of the steady-state fluorescence spectra yielded I_E/I_M ratios of 0.68 and 5.65 for the sample in DMSO and water, respectively. The close to 10-fold increase in I_E/I_M from DMSO to water indicates that more excimer is formed in water. This observation was further substantiated by acquiring time-resolved fluorescence decays. As for the fluorescence spectra, changing the

solvent from DMSO to water had a profound effect on the fluorescence decays of the pyrene monomer and excimer. The fluorescence decay of the pyrene monomer was quasi monoexponetial in DMSO with an average lifetime $<\tau>$ equal to 50 ns. The decay of the pyrene monomer in water was much shorter-lived with a $<\tau>$ value of 17 ns, reflecting a more efficient excimer formation as would be expected if the hydrophobic pyrene labels were to cluster at the centre of the PAB(5)-SNP0 particles to minimize their exposure to water. Pyrene aggregation could also be inferred from the appearance of the excimer decays. In DMSO where pyrene is soluble, the excimer decays showed a pronounced rise time reflecting the time spanned between the excitation of a pyrene monomer and its encounter with a ground-state pyrene. In water, no risetime was observed demonstrating the existence of ground-state pyrene aggregates that emitted instantaneously upon excitation of the solution. The results of the fluorescence decay analysis were shown in Tables 4.1 and 4.2. In Table 4.2, $<k>$ is the average quenching rate constant, and f_{diff}, f_{free}, and f_{agg} are the molar fractions of pyrene labels that form excimer via diffusion, are isolated and never form excimer, and are associated and form excimer instantaneously upon direct excitation, respectively. In DMSO, 80% of the excimer was formed by diffusion, while in water, 95% of the excimer is generated though the direct excitation of aggregated pyrene pendants. The rate constant of excimer formation is 5 times larger in water than in DMSO.

Table 4.1. Pre-exponential factors and decays times retrieved from the Model Free Analysis of the fluorescence decays of PBA(5)-SNP0 in DMSO and water using the analysis program sumegs7-4bg

Monomer	a_1	τ_1 (ns)	a_2	τ_2 (ns)	a_3	τ_3 (ns)	a_M	τ_M (ns)	a_S	τ_S (ns)	χ^2
DMSO	0.22	20.7	0.63	60.8	_	_	0.02	100	0.09	3.5	1.03
Water	0.54	5.1	0.34	19.1	0.10	76.8	0.02	150	_	_	1.03

Excimer	f_{Ediff}	f_{EE0}	τ_{E0} (ns)	f_{EEL}	τ_{EL} (ns)	a_S	τ_S (ns)	χ^2
DMSO	0.72	0.16	43.9	_	_	0.12	3.5	1.03
Water	0.03	0.50	44.2	0.11	80.7	0.36	3.5	1.03

Table 4.2. Results from the model free analysis of the fluorescence decays of PBA(5)-SNP0 in both DMSO and water.

Solvent	$\eta \frac{@25^\circ C}{mPa.s}$	I_E/I_M	<k>, μs^{-1}	f_{diff}	f_{free}	f_{agg}
DMSO	1.99	0.68	9.8	0.80	0.02	0.18
Water	0.89	5.65	52.1	0.05	0.00	0.95

The higher viscosity of DMSO which also reduces pyrene excimer formation by diffusion can be accounted for by considering the product of the rate constant for excimer formation and

the solvent viscosity, namely $\langle k \rangle \times \eta$. $\langle k \rangle \times \eta$ is 2.4 times larger in water than in DMSO, confirming the efficient excimer formation for the PBA(5)-SNP0 in water.

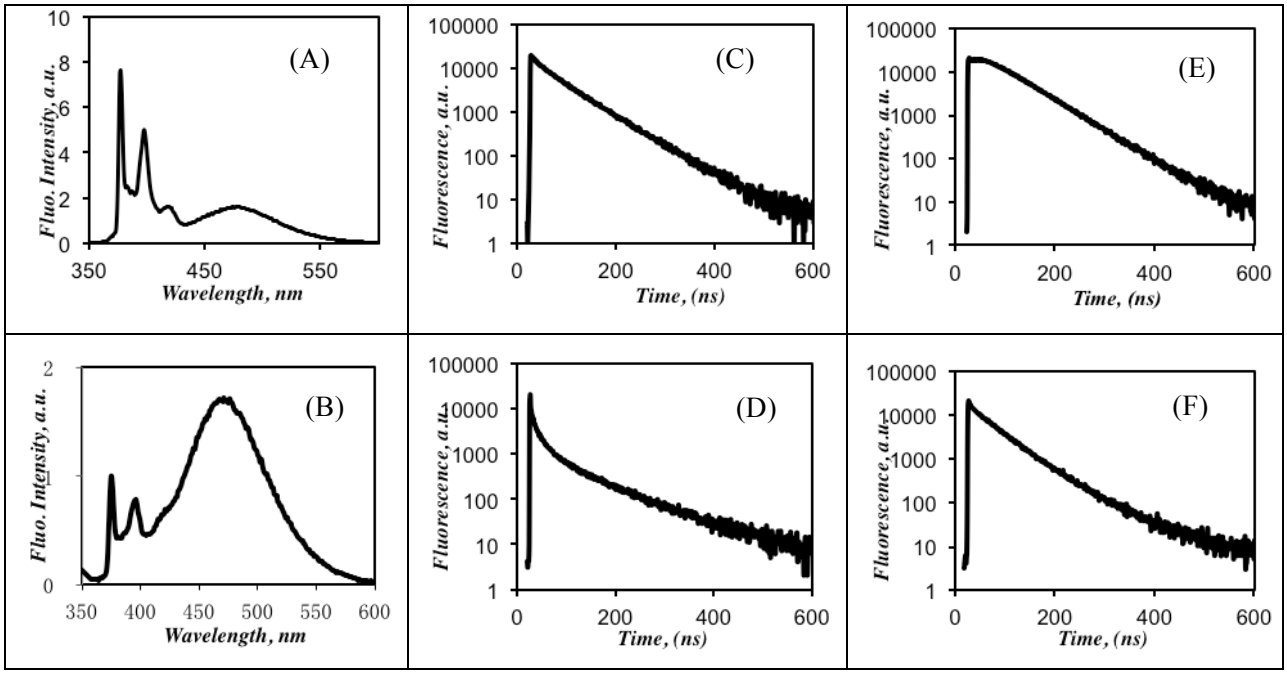

Figure 4.5. Steady-state fluorescence spectra (λ_{ex}=344 nm) for PBA(5)-SNP0 in (A) DMSO and (B) water (λ_{ex}=344 nm, λ_{em}=375 nm) and time-resolved fluorescence decays of the pyrene monomer in (C) DMSO and (D) water and of the pyrene excimer in (E) DMSO and (F) water.

The results presented in Figure 4.5 illustrate the importance of the hydrophobic effect on the behavior of pyrene. In water, the pyrene molecules tend to aggregate with each other in order to reduce their interactions with water. Pyrene aggregation reduces the surface area of the hydrophobic pyrene being exposed to water. Whereas pyrene aggregation in water is clearly demonstrated by steady-state and time-resolved fluorescence, there is still a limited

understanding of how it might affect the conformation of the whole particle. Such information can be obtained from TEM measurements.

4.3.4 Characterization of PBA(5)-SNP0 by TEM

The morphology and size distribution of PBA(5)-SNP0 were determined through the analysis of TEM images. The fluorescence results shown in Figure 4.5 indicate that PBA(5)-SNP0 behaves quite differently in DMSO than in water. In turn, these differences which were probed at the molecular level by monitoring the fluorescence of pyrene are expected to also affect the conformation adopted by PBA(5)-SNP0 in DMSO and water. Since DMSO is a good solvent for starch and pyrene, PBA(5)-SNP0 in DMSO should exhibit the same spherical shape observed for the unlabeled SNPs in DMSO or water. However, the hydrophobic collapse undergone by the pyrene-labeled particles where the pyrene labels aggregate toward the centre of the particle, should affect the morphology of the particle. TEM was employed in an effort to assess the effect that the hydrophobic pyrene labels had on the size of individual SNPs as a function of solvent polarity. To this end, TEM images were acquired for the unlabeled SNPs and PBA(5)-SNP0 prepared from solutions in water and DMSO and stained with RuO_4. DMSO is a good solvent for both starch and pyrene. In DMSO, PBA(5)-SNP0 was stained homogenously with RuO_4, and showed a spherical shape (see Figure 4.6B), similar to that of the unlabeled SNPs in DMSO and water (see Figure 4.7). In water however, PBA(5)-SNP0 showed a unique core-shell morphology which was attributed to the aggregation of the hydrophobic pyrenes that clustered toward the centre of PBA(5)-SNP0 to minimize their exposure to water. The darker zone formed at the centre of the pyrene-labeled particles reflects the stronger binding of RuO_4 to the pyrene

labels that aggregate at the core of the particles or merely enhanced the density of starch at the centre of the particles due to the hydrophobic collapse of the pyrene-labeled strands of the SNPs. Whatever the reason for the enhanced staining of the PBA(5)-SNP0 core by RuO_4 in water, both interpretations reflect the hydrophobic collapse of the particles due to the presence of pyrene.

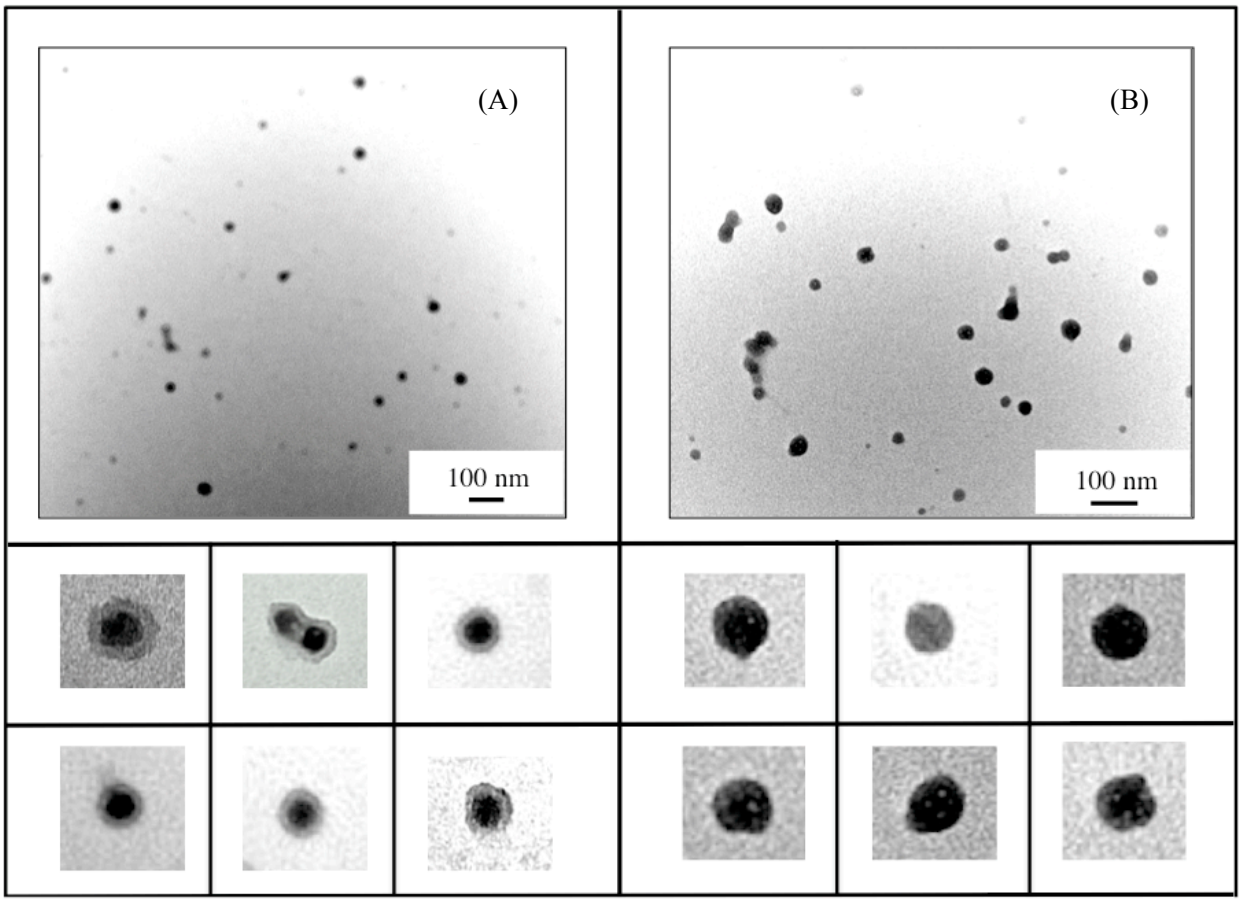

Figure 4.6. TEM images of the PBA(5)-SNP0 sample prepared from (A) DMSO and (B) water

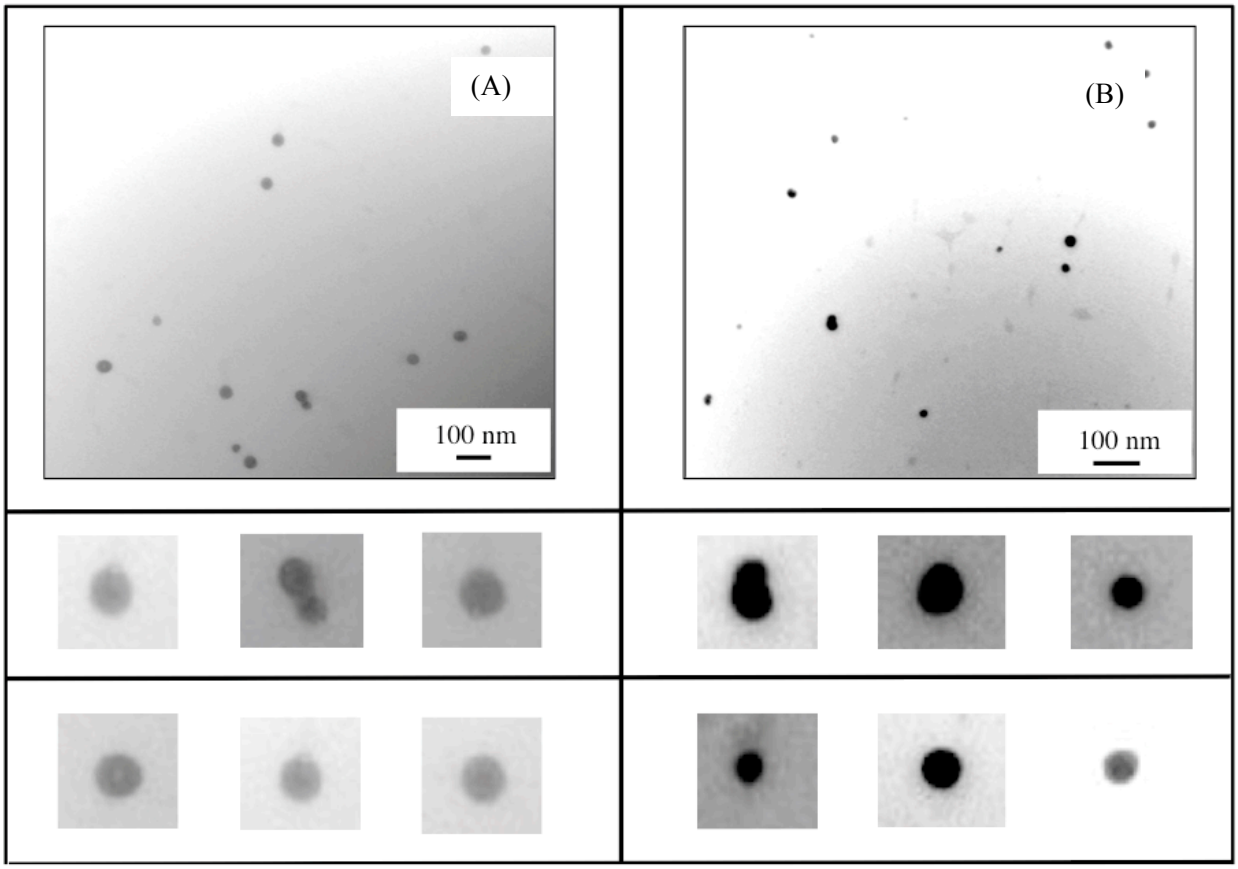

Figure 4.7. TEM images of SNP0 prepared from (A) DMSO and (B) water.

The hydrophobic collapse undergone by PBA(5)-SNP0 was further investigated by analyzing the size distribution of the particles shown in Figures 4.6 and 4.7. To this end, a minimum of 40 particles were selected in the TEM images and their diameter was measured to generate an histogram. Figure 4.8A and B shows the histograms obtained from the TEM images. These histograms led to the conclusion that the PBA(5)-SNP0 particles have an average diameter of 30 ± 14 nm and 20 ± 9 nm in DMSO and water, respectively. The diameter of the core of the pyrene-labeled particles was determined from the images and found to equal 13 ± 5 nm.

Interestingly, the collapsed conformation adopted by the hydrophobically modified particles in water was retained after water had evaporated from the TEM grid for the TEM images, possibly due to the stiffness of the highly branched amylopectin.[32]

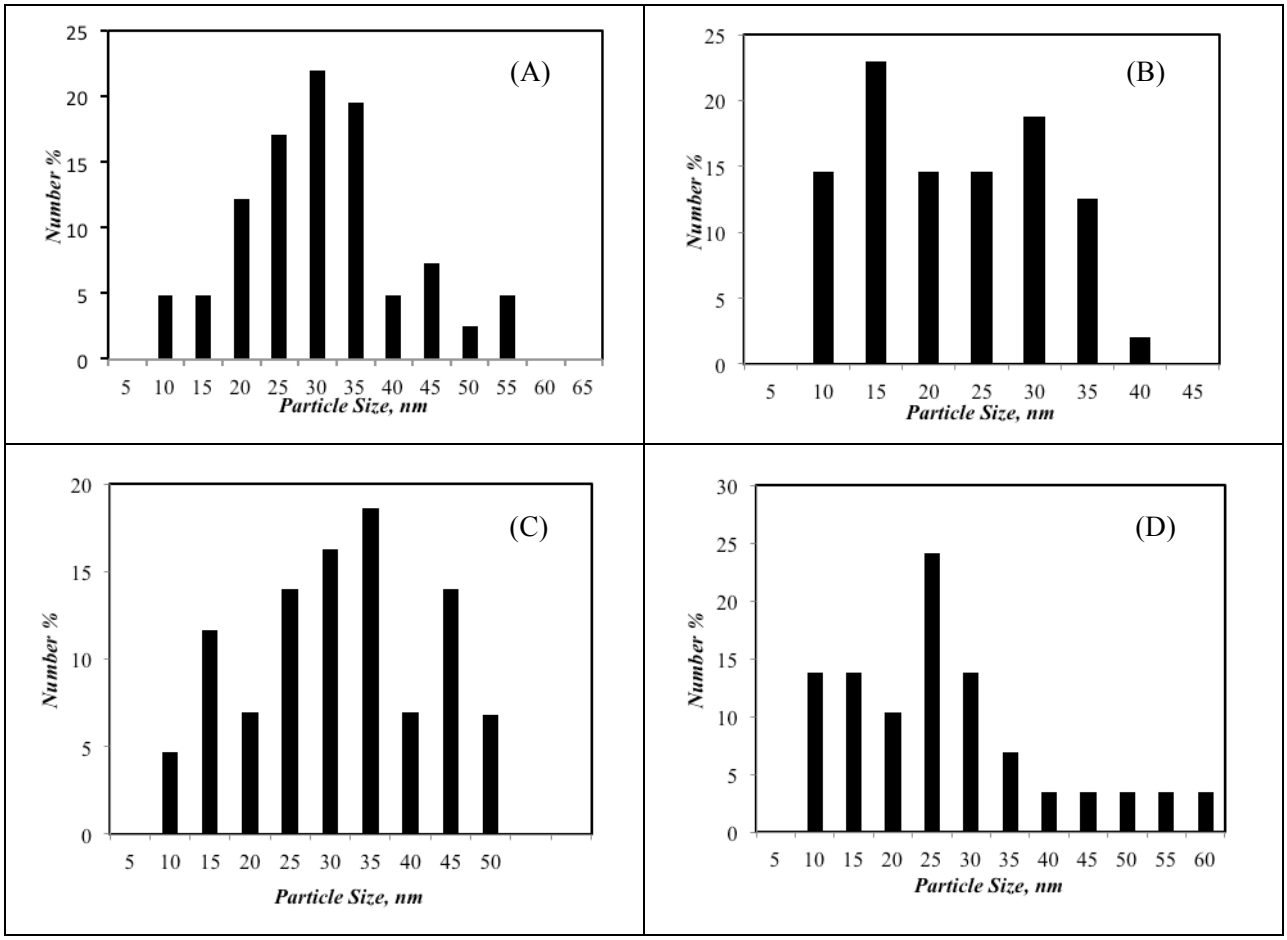

Figure 4.8. Particle size distribution determined from the TEM image of (A) PBA(5)-SNP0 in DMSO, (B) in water, (C) SNP0 in DMSO and (D) SNP0 in water.

Figure 4.8C and D were obtained from unlabeled SNP0 prepared in DMSO and water, respectively. SNP0 prepared in DMSO had an average diameter of 29 ± 11 nm while SNP0

prepared in water had an average size of 24 ± 10 nm. From the TEM measurements, the PBA(5)-SNP0 particles had a diameter in DMSO and water that was similar to that of the unlabeled SNP0. The main difference was the core-shell structure observed uniquely in water for PBA(5)-SNP0, a clear indication of the aggregation of the pyrene labels toward the center of the SNPs. The size distribution of PBA(5)-SNP0 in DMSO obtained from the TEM image was also compared with the D_h histogram generated from DLS as shown in Figure 4.9.

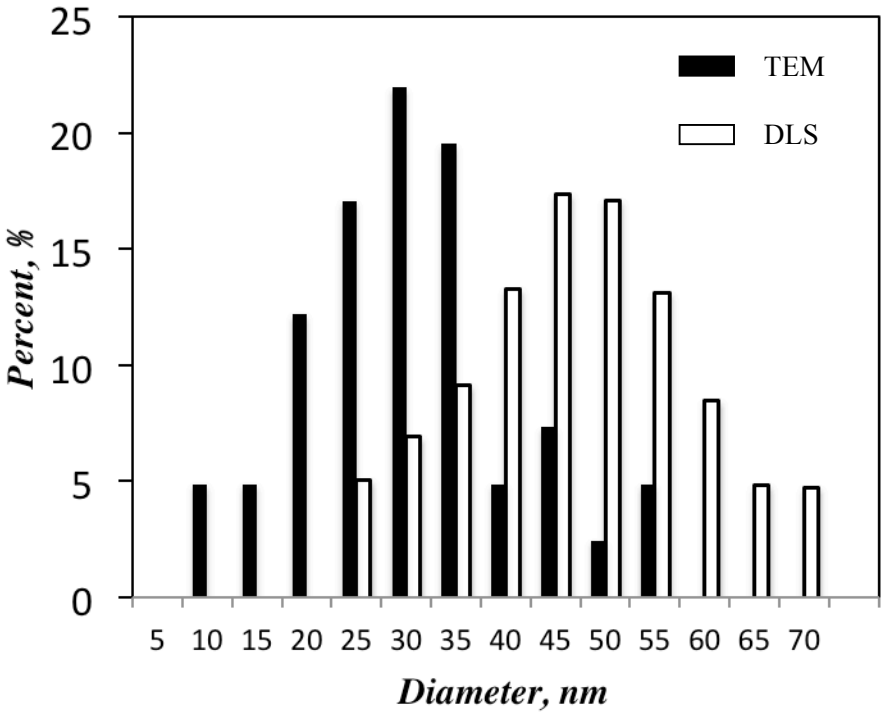

Figure 4.9 Particle size distribution of PBA(5)-SNP0 determined from TEM image (filled bars) and DLS (unfilled bars) in DMSO.

The hydrodynamic diameter of the solvated SNPs obtained from DLS is larger than the diameter of the dry SNPs determined from the TEM image. D_h from DLS was found to equal 49 ± 9 nm

whereas the diameter of the dry particles equaled 30 ± 14 nm. The increase in the diameter observed by DLS reflects the swollen nature of the particles in solution.

4.4 Conclusions

Pyrene excimer formation was used to probe the local pyrene concentration $[Py]_{loc}$ inside the Py-SNPs as the particles were subject to external stresses induced by the presence of a large number of unlabeled particles in the semi-dilute regime or the use of water as a solvent to induce the hydrophobic collapse of those strands bearing a pyrene label. In the semi-dilute regime, Py-SNPs underwent a contraction probably because the branched and rigid structure of amylopectin that constitutes the SNPs prevents their entanglement as would be normally observed for linear polymers. In water, fluorescence measurements demonstrated the aggregation of the hydrophobic pyrene labels which led to a core-shell structure for the particles as demonstrated by transmission electron microscopy.

Chapter 5

Conclusions and Future Work

5.1 Conclusions

The main aim of this project was to characterize the solution behavior of SNPs in an effort to understand their excellent performance in paper coating applications. Based on the predicted structure of the SNPs being porous and highly swellable nanogels made of crosslinked chains of branched amylopectin, a set of fluorescence experiments were initiated where the SNPs would be fluorescently labeled and quenched with a polymeric quencher. By monitoring the quenching efficiency of the fluorescently labeled SNPs with polymeric quenchers of different molecular sizes, fluorescence protective quenching experiments were expected to provide a measure of the pore size of the SNPs. To achieve these goals, the project was divided into three parts.

The first part described in Chapter 2 of this thesis illustrates how the SNPs were fluorescently labeled with the hydrophobic dye pyrene. The labeling protocol was initially based on the nucleophilic attack of 1-pyrenemethylenechloride by alkoxides generated by the deprotonation of the starch hydroxyls, and as such proceeded under basic conditions. Sodium hydride used to deprotonate the starch hydroxyls was found to be too strong a base which led to the degradation of the SNPs as demonstrated from the smaller hydrodynamic diameters obtained for the SNPs after reaction. The same reaction was attempted with the weaker base dimethylaminopyridine (DMAP). While these reaction conditions did not degrade the SNPs, they resulted in the covalent attachment of only minute amounts of pyrene. These disappointing results led us to try another approach where 1-pyrenebutanoic acid would be coupled with diisopropylcarbodiimide (DIC) in the presence of DMAP. This approach turned out to be highly successful, yielding pyrene-labeled SNPs whose dimension was preserved according to DLS

measurements conducted in DMSO where pyrene was soluble and with pyrene content that could be adjusted between 0.5 and 5 mol%. ^{1}H NMR, UV-Vis spectroscopy, and fluorescence were applied to confirm the chemical composition of the different products and reaction intermediates.

Having established a reliable synthetic procedure to fluorescently label the SNPs with 1-pyrenebutyric acid, Chapter 3 dealt with the synthesis of the polymeric quencher. The hydroxyl end of a 2K poly(ethylene glycol) terminated at the other end with a methyl group (Me-PEG-OH) was modified with either a pyridinium chloride or a nitropropane substituent, both being known quenchers of pyrene. The synthesis of the pyridinium terminated Me-PEG construct was rapidly abandoned as it was found to degrade over time. The nitro-terminated Me-PEG polymeric quencher was obtained by forming a peptide bond between Me-PEG-NH_2 and nitropropionic acid. To this end, the terminal hydroxyl of Me-PEG-OH was replaced by an amine, first by reducing an azide group covalently attached to the Me-PEG terminal by nucleophilic attack of the chlorinated end of Me-PEG-Cl by an azide anion, and second by applying the Mitsunobu reaction to Me-PEG-OH. This last synthesis afforded a reliable and easier synthetic route to prepare Me-PEG-NH_2 which was then coupled to nitropropionic acid using DIC and hydroxybenzotriazole to obtain Me-PEG-C_3NO_2. The polymeric quencher was then applied to quench the pyrene-labeled SNPs (Py-SNPs). While the fluorescence of pyrene was quite efficiently quenched by nitromethane, the loss in translational mobility experienced by the large Py-SNPs and Me-PEG-NO_2 was so massive that high concentrations of polymeric quencher were required to induce any detectable quenching of fluorescence by diffusive encounters between the Py-SNPs and Me-PEG-NO_2. Unfortunately, the large concentrations of

Me-PEG-NO_2 meant that the residual absorption of the polymeric quencher at 346 nm where pyrene absorbs became significant and prevented the fluorescence quenching experiments of the Py-SNPs by the selected polymeric quencher. As a result, this line of research was discontinued and the report focused instead on the characterization of the SNPs by monitoring the process of intramolecular pyrene excimer formation within the Py-SNPs. This led to the set of experiments conducted with steady-state and time-resolved fluorescence and transmission electron microscopy described in Chapter 4.

The proportionality that exists between the I_E/I_M ratio and the local pyrene concentration was taken advantage of to probe how the volume of the Py-SNPs would respond when different stresses were applied to them, as an expansion or contraction in volume would result in a decrease or increase in the I_E/I_M ratio, respectively. To this end, a small quantity of Py-SNP was added to concentrated solutions of non-fluorescent SNPs and the I_E/I_M ratio was monitored as a function of SNP concentration. Surprisingly, the I_E/I_M ratio was found to increase with increasing SNP concentration, demonstrating a decrease in the SNP volume. It appeared that instead of entangling through interpenetration with other SNPs as linear polymers would do in the semi-dilute regime, the rigid and branched SNP interior prevented the interpenetration of the particles and led to their contraction. The deformability of the SNPs was also illustrated by studying the structure of the Py-SNPs in water where the hydrophobic pyrene labels randomly distributed throughout the particles aggregated in the particle center, thus generating a core-shell structure that was demonstrated by TEM. The core-shell structure was only observed for the Py-SNPs in water where the hydrophobic effect resulted in the sequestering of the pyrene labels at the

particle center. In DMSO, the particles showed a homogeneous density throughout. The demonstration that pyrene excimer formation can probe at the molecular level how the SNPs deform under various conditions opens the path to numerous experiments that will characterize the stiffness and propensity to deform of these particles.

5.2 Future Work

This thesis has provided an important analytical tool to probe the expansion or compression of SNPs at the molecular level. In turn, the ability of SNPs to deform might represent a key factor to explain the excellent performance of SNP solutions in paper coating applications. Since large SNPs have been shown not to be able to penetrate the interior of Py-SNPs, it will be interesting to investigate if smaller macromolecules, such as linear PEO chains could penetrate the interior of Py-SNPs. By comparing the profiles of the I_E/I_M ratio versus PEO concentration for different PEO chains, conditions might be found where short PEO chains can diffuse inside the Py-SNPs and reduce the I_E/I_M ratio. In so doing, the accessibility of the SNP interior could be evaluated based on the known size of a PEO coil in solution. The accessibility of the SNP interior could also be probed as a function of the size of other SNPs, since smaller SNPs might be able to penetrate the interior of larger SNPs. This would be accomplished by monitoring the I_E/I_M ratio of a large Py-SNP as a function of the concentration of a small SNP. If interpenetration happens, these experiments would suggest that a formulation containing a broad distribution of SNP sizes would be valuable for film formation as it would allow the smaller SNPs to penetrate the interior of the larger SNPs, thus resulting in better film formation. This represents a small sample of the numerous experiments that can be developed based on this effect.

References

1. Le Corre, D.; Bras, J.; Dufresne, A. Starch Nanoparticles: A Review. *Biomacromolecules* **2010**, *11,* 1139-1153.

2. Hoover, R. Composition, Molecular Structure, and Physicochemical Properties of Tuber and Root Starches: a Review. *Carbohydrate Polym*. **2001**, *45*, 253-267.

3. Bertoft, E.; Piyachomkwan, K.; Chatakanonda, P.; Siroth, K. Internal Unit Chain Composition in Amylopectins. *Carbohydrate Polym*. **2008**, *74*, 527-543.

4. Bloembergen, S.; McLennan, I. J.; van Leeuwen, J.; Lee, D. I. Specialty Biobased Monomers and Emulsion Polymers Derived from Starch. *PTS Advanced Coating Fund. Symp., Munich, Oct.* 11-14, **2010**.

5. Brown, W. H.; Poon, T. *Introduction to Organic Chemistry* (3rd ed.), Wiley, **2005**.

6. Lee, D. I.; Blombergen, S.; Van Leeuwen, J. Development of New Biobased Emulsion Binders. *PaperCon, TAPPI,* **2010**.

7. Winnik, F. M. Photophysics of Preassociated Pyrenes in Aqueous Polymer Solutions and in Other Organized Media. *Chem*. *Rev*. **1993**, *301*, 1019-1027.

8. Duhamel, J. Internal Dynamics of Dendritic Molecules Probed by Pyrene Excimer Formation. *Polymers* **2012**, *4*, 211-239.

9. Duhamel, J. Molecular Interfacial Phenomena of Polymers and Biopolymers. *Woodhead Publishing Limited*: Cambridge, England, 2005; pp216-222.

10. Duhamel, J. Polymer Chain Dynamics in Solution Probed with a Fluorescence Blob Model. *Acc. Chem. Res.* **2006**, *39*, 953-960.

11. Duhamel, J. New Insight in the Study of Pyrene Excimer Fluorescence to Characterize Macromolecules and their Supramolecular Assemblies in Solution. *Langmuir* **2012**, *28*, 6527-6538.

12. Duhamel, J. Global Analysis of Fluorescence Decays to Probe the Internal Dynamics of Fluorescently Labeled Macromolecules. *Langmuir* **2014**, 30, 2307-2324.

13. Berlman, I. B. *Handbook of Fluorescence Spectra of Aromatic Molecules*. Academic Press, Inc.: New York, **1971**, 383.

14. Birks, J. B. *Photophysics of Aromatic Molecules*. Wiley: New York, **1970**, 301.

15. Cuniberti, C.; Perico, A. Intramolecular Excimer Formation in Polymers: Pyrene Labelled Poly(vinyl acetate). *Eur. Polym. J.* **1980**, *16,* 887-893.

16. Lakowicz, J. R. *Principles of Fluorescence Spectroscopy* (1st ed). **1983**, 280-281.

17. Winnik, M. A. End-to-End Cyclization of Polymer Chains. *Acc. Chem. Res.* **1985**, *18*, 73-79.

18. Cuniberti, C.; Perico, A. Intramolecular Excimers and Microbrownian Motion of Flexible Polymer Molecules in Solution. *Eur. Polym. J.* **1977**, *13,* 369-374.

19. Guan, Y.; Qian, L.; Xiao, H.; Zheng, A. Preparation of Novel Antimicrobial-Modified Starch and its Adsorption on Cellulose Fibers: Part I. Optimization of Synthetic Conditions and Antimicrobial Activities. *Cellulose* **2008**, *15,* 609-618

20. Winnik, F. M.; Winnik, M. A.; Tazuke, S.; Ober, C. K. Synthesis and Characterization of Pyrene-Labeled Hydroxypropyl Cellulose and its Fluorescence in Solution. *Macromolecules* **1987**, *20*, 38-44.

21. Held, I.; von den Hoff, P.; Stephenson, D. S.; Zipse, H. Domino Catalysis in the Direct Conversion of Carboxylic Acids to Ester. *Adv. Synth. Cat.* **2008**, *11,* 1891-1900.

22. Neises, B.; Steglich, W. Simple Method for the Esterification of Carboxylic Acids. *Angew. Chem. Int. Ed.* **1978**, *17,* 522-524.

23. Hachmann, J. Search of Optimal Coupling Reagent in Multiple Peptide Synthesizer. *Biopolymers* **2006**, *84*, 340-347

24. Jankova, K.; Kops, J. ^{1}H NMR Investigation of Quantitative Fuctionalization of Poly(ethylene glycol)s. *J. Appl. Polym. Sci.* **1994**, *54,* 1027-1032.

25. Dust, J. M.; Fang, Z. H.; Harris, J. M. Proton NMR Characterization of Poly(ethylene glycols) and Derivatives. *Macromolecules* **1990**, *23*, 3742-3746.

26. Viscardi, G.; Quagliotto, P.; Barolo, C.; Savarino, P.; Barni, E.; Fisicaro, E. Synthesis and Surface and Antimicrobial Properties of Novel Cationic Surfactants. *J. Org. Chem.* **2000**, *65,* 8197-8203.

27. Lin, F. L.; Hoyt, H. M.; v. Halbeek, H.; Bergman, R. G.; Bertozzi, C. R. Mechanism Investigation of Staudinger Reaction. *J. Am. Chem. Soc*. **2005**, *127*, 2686-2694.

28. Mitsunobu, O. The Use of Diethyl Azodicarboxylate and Triphenylphosphine in Synthesis and Transformation of Natural Products. *Synthesis* **1981**, *1*, 1–28.

29. Bodanszky, M. *Peptide Chemistry: A Practical Text Book* (2nd ed.); Springer: Verlag Berlin, **1993**.

30. Montalbettim, C. A. G. N.; Falque, V. Amide Bond Formation and Peptide Coupling. *Tetrahedron* **2005**, *61,* 10827-10852.

31. Winnik, F. M. Phase Transition of Aqueous Poly-(*N*-isopropylacrylamide) Solution: A Study by Non-Radiative Energy Transfer. *Polymer* **1990**, *31*, 2125-2134.

32. Gai, X. S.; Coutifaris, B. A.; Brewer, S. H and Fenlon, E. E. A Direct Comparison of Azide and Nitrile Vibrational Probes. *Phys*. *Chem. Chem. Phys.* **2011**, *13*, 5926-5930.

33. Mueller, E.; Blume, A. FTIR Spectroscoic analysis f the amide and acid bands of ganglioside G_{m1}, in Pure Form and in Mixtures with DMPC. *Biochim. Biophys. Acta.* **1993,** *1146,* 45-51

34. Charles, T. *The Hydrophobic Effect: Formation of Micelles and Biological Membranes* (2d ed.). New York: Wiley **1980**.

35. Charles, T. The Hydrophobic Effect and the Organization of Living Matter. *Science* **1978**, *200,* 1012-1018.

36. Froehling, P. E.; Pijpers, A. J. Ruthenium Tetroxide as a Staining Agent for Transmission Electron Microscopy of Polyamide-Polyether Blends and Block Copolymers. *J. Polym. Sci. B: Polym. Phys.* **1987**, *25*, 947-952.

37. Irondi, K.; Zhang, M. Z.; Duhamel, J. Study of the Semidilute Solutions of Poly(*N,N*-dimethylacrylamide) by Fluorescence and Its Implications to the Kinetics of Coil-to-Globule Transitions. *J. Phys. Chem. B* **2006**, *110*, 2628-2637.